

Monitoring Waterflood Front Movement by Propagating High Frequency Pulses through Subsurface Transmission Lines

Jesus M. Felix Servin

Abstract /

This article describes a novel approach to monitor waterflood front movement using proximity sensing in conjunction with contrast agents. Our technique exploits the presence of resistive layers between reservoirs, which act as a transmission line for electromagnetic (EM) signals, to achieve increased propagation range. This work focuses on numerical simulations to evaluate the potential of this approach to monitor water movement in the reservoir under different conditions.

A series of 2D axisymmetric numerical simulations were conducted to assess the potential of proximity sensing to monitor moving fronts of labeled brine as well as to detect isolated pockets of brine labeled with contrast agents. The study was conducted using layered models that resemble a resistive seal bounded by reservoirs saturated with brine or brine and contrast agents. The effect of magnetic permeability (μ) on signal traveltime and amplitude is reported and compared to the effect of electric permittivity (ϵ).

The results show that proximity sensing is a suitable technique to detect changes in the μ of reservoirs adjacent to resistive seals. Therefore, our approach can be used in combination with contrast agents, such as magnetic nanomappers, to monitor waterflood front movement in the reservoir. In addition, this technique can be used to detect isolated pockets of labeled brine, which suggests that injection of slugs of labeled water would be enough for field applications. The observed effect of the μ on signal traveltime is similar to the trend observed when the ϵ of the bounding reservoirs is changed. A significant difference is that increasing the μ of the bounding reservoirs appears to reduce signal amplitude, while increasing the ϵ has the opposite effect. This result was unexpected and requires further simulations and experimentation to validate this behavior.

Proximity sensing offers a novel approach to address the challenge of EM propagation in conductive media and paves the way for the development of refined techniques that provide reservoir saturation and waterflood front monitoring capabilities with greater resolution.

Introduction

Reservoir saturation mapping and waterflood front monitoring are ongoing goals for reservoir engineering toward the development of enhanced production and injection strategies. Current tools include reservoir models based on seismic data, well logs and production data to provide vital information toward that end. Consequently, there is a need for new methods to monitor the reservoir in real-time, and provide information on accurate saturation and reservoir fluid movement.

Two main approaches have been used to characterize and monitor the reservoir: (1) seismic and electromagnetic (EM) surveys, and (2) 4D seismic, which has been successfully used to monitor clastic reservoirs around the world¹⁻⁴. Subsequently, its implementation has been limited in other kinds of reservoirs, due to the poor acoustic impedance between brine and water⁵. EM approaches, such as cross-well EM⁶, borehole to surface induced polarization⁷⁻⁹, and surface to borehole EM¹⁰ have been successfully used to map saturation in carbonate reservoirs. Traditional EM approaches rely on the use of low frequencies — up to hundreds of Hz — to achieve depths of investigation in the order of hundreds of meters. Although, the low frequencies result in low intrinsic resolution, and therefore, these methods are better suited to image large features. Therefore, new approaches with improved resolution are needed to detect smaller features. A method that provides saturation mapping and waterflood front monitoring capabilities is indeed highly desirable.

Proximity sensing has been previously proposed as a way to significantly increase the depth of penetration of high frequency cross-well EM surveys for saturation mapping¹¹⁻¹³. This method, which is similar to radio imaging technology used in the mining industry¹⁴, is applicable for reservoirs with resistive seals (such as evaporites). In brief, proximity sensing exploits the presence of resistive reservoir seals to propagate high frequency EM pulses that are modulated by the EM properties of the bounding reservoirs, which are dependent on the fluid saturation.

In this way, proximity sensing addresses the challenge of long-range EM propagation at high frequencies, and paves the way for refined reservoir saturation surveys. Previous simulations and experimental results support our claim that proximity sensing is sensitive to changes in the electric permittivity (ϵ) of the reservoir, and therefore can be effectively used to differentiate between brine-saturated and oil-saturated regions in the reservoir.

The use of superparamagnetic nanoparticles as contrast agents to label injected water used in combination with EM surveys has been previously proposed as a way to monitor waterflood front movement in real time¹⁵. This work strives to analyze the possibility of using such contrast agents, e.g., magnetic nanomappers, in combination with proximity sensing to develop an improved approach to waterflood front monitoring.

Simulations

To evaluate the possibility of using proximity sensing in conjunction with magnetic nanomappers or any other magnetic contrast agent to monitor waterflood movement, a series of 2D axisymmetric transient EM numerical simulations were performed using a commercially available finite element modeling package. The models consist of a central layer representing an evaporite seal bounded by two layers representing reservoirs saturated with brine or brine and magnetic contrast agents, Fig. 1. All models measure 500 m in length and 230 m in height. The seal layer is 30 m thick and the reservoir layers are each 100 m thick. The maximum mesh element size was defined such that there were at least 10 elements per wavelength. The transmitter (Tx) and receiver (Rx) were placed on the left and right edge of the model, respectively, inside the seal layer.

The EM source was modeled as a dipole antenna

Fig. 1 Model schematic and dimensions. The black dots represent the approximate location of the transmitter (left) and receiver (right).



consisting of two hollow metallic arms, each one 7.5 m in length with a resonant frequency of 4.47 MHz — wavelength of 30 m in free space. The model accounts for resistive losses and finite conductivity. The power supply was not explicitly modeled. Instead, the antenna was excited by applying a modulated Gaussian pulse with a fundamental frequency of 4.47 MHz, Fig. 2, across the faces of the antenna arms. The frequency was chosen such that the resulting wavelength would be comparable to the thickness of the seal layer. The Tx was located along the left edge of the model, centered vertically within the evaporite seal layer, Fig. 1. The Rx was not explicitly modeled, instead, a point probe was used to measure the electric field norm as a function of time.

Results and Discussion

Effect of Magnetic Contrast Agents

The first set of simulations were performed to investigate the effect of magnetic permeability (μ) contrast agents on

Fig. 2 Transient voltage pulse used to drive the antenna.



signal traveltime and amplitude. Three different scenarios were considered. In scenario 1, both reservoirs were brine saturated; in scenario 2, the lower reservoir was saturated with brine + contrast agents (labeled brine);

in scenario 3, both reservoirs were saturated with brine + contrast agents, Fig. 3.

If changes in the μ of the formation have a similar effect to that of changes in the ϵ , one should expect scenario 3 to result in the shortest traveltime, followed by scenario 2 and then scenario 1. This is because increasing the μ , ϵ , and conductivity of the bounding layers should result in better signal containment within the seal layer, through which the signal propagates faster due to its EM properties, Table 1.

The results show that adding magnetic contrast agents to the bounding reservoirs reduces the signal traveltime. As expected, scenario 3 results in the shortest traveltime, while scenario 1 results in the longest traveltime, Fig. 4. This suggests that the μ contrast agents can be used to create unique signatures in the reservoir for EM surveys. The effect of increasing the μ of the surrounding layers appears to be similar to what has been reported for increasing the ϵ of the surrounding layers¹¹⁻¹³, both resulting in shorter traveltimes. An unexpected result is the relatively low amplitude of the received signal for scenario 2 and 3 compared to scenario 1.

Previous simulations and experiments¹¹⁻¹³ suggest that bounding reservoirs with high values of the ϵ and

Fig. 3 Models used to evaluate the effect of the μ on traveltime. The sections colored in blue represent a brine saturated reservoir; the sections colored in gold represent a reservoir saturated with labeled brine. The axis of symmetry is along the left edge of the models.

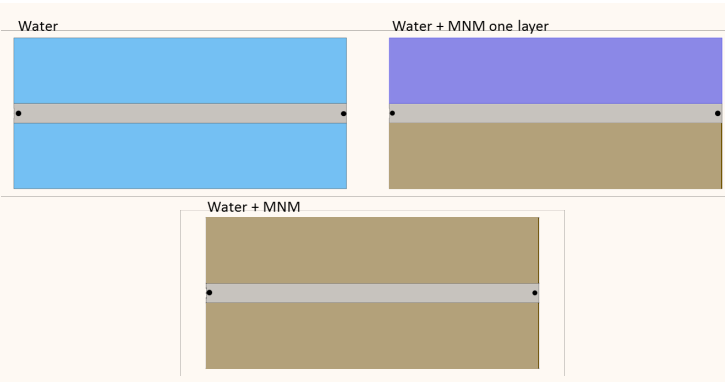
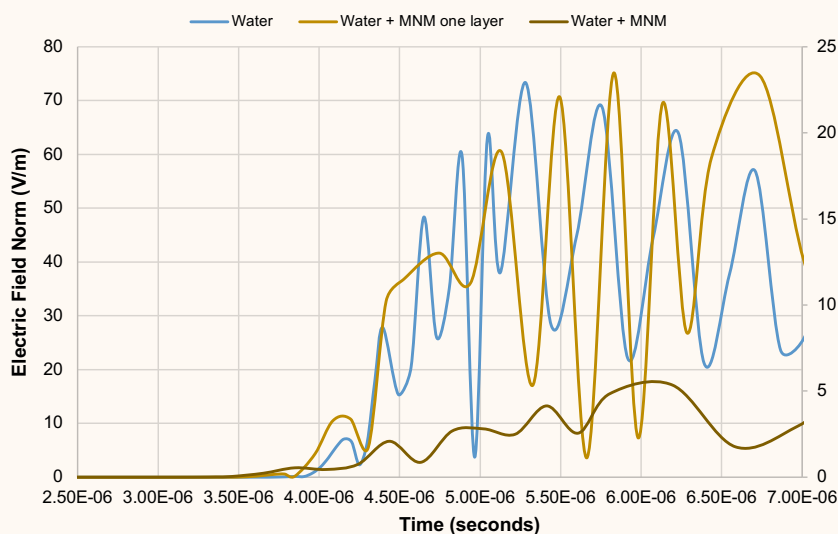


Table 1 EM properties of each layer.

Formation	μ_r	ϵ_r	σ [S/m]
Evaporite seal	1	5	0.0001
Reservoir saturated with brine	1	14	0.38
Reservoir saturated with brine + magnetic contrast agents	2	14	0.38

Fig. 4 Received transients for the models used to evaluate the effect of the μ on traveltime. The results show that adding labeled brine to the adjacent reservoirs reduces traveltime. Water + MNM one layer and Water + MNM are plotted on the secondary vertical axis.



conductivity would prevent the signal from escaping the seal layer, which is highly resistive, and therefore acts as a low-loss channel. As a result, the higher the ϵ and conductivity of the bounding layers, the greater the received signal amplitude. Subsequently, the simulation results show a significant drop in amplitude when the μ contrast agents were added to one or both of the bounding reservoirs, Fig. 4.

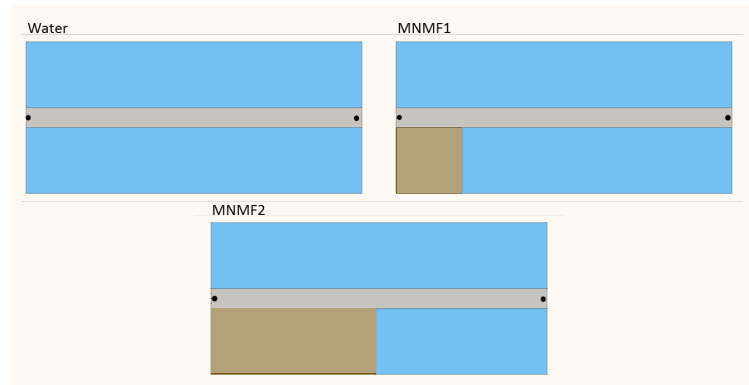
These results will have to be confirmed through laboratory experiments and further simulations. At this point it is not clear why increasing the m would have such an effect on signal amplitude.

Waterflood Front Mapping Using Proximity Sensing and the μ Contrast Agents

Given that increasing the μ has a significant effect on traveltime, the possibility of using the μ contrast agents to label injected water was investigated. Three different scenarios were considered for this purpose: in scenario 1, both reservoirs are saturated with brine; in scenario 2 and 3, a front of magnetically labeled water is present in the bottom reservoir, Fig. 5.

Based on the results shown so far, adding the μ contrast agents to the reservoir should result in a shorter traveltime. Following that logic, scenario 3 should be the fastest and scenario 1 the slowest. The results confirm the trend observed before, the larger the magnetically labeled water front is, the shorter the traveltime, Fig. 6. These results were expected and support the hypothesis that the μ has a similar effect to that of the ϵ on traveltime for this system. It is worth mentioning that the larger front results on a significant signal amplitude reduction, similar to what was observed when the entire reservoir was saturated with labeled brine. It is unclear what could be causing this drop, and laboratory experiments and additional simulations will be required to confirm such behavior.

Fig. 5 Models used to evaluate the sensitivity of proximity sensing to moving fronts of labeled brine. The sections colored in blue represent a brine saturated reservoir; the sections colored in gold represent a reservoir saturated with labeled brine. The axis of symmetry is along the left edge of the models.



The possibility of detecting isolated pockets of magnetically labeled water was also investigated. The pocket size was varied from 30 m to 120 m in 2x steps to investigate the effect on signal traveltime and amplitude, Fig. 7. According to our hypothesis, the larger the pocket of labeled water, the shorter the traveltime due to signal containment within the sealed layer.

The simulation results showed the expected trend: the model having the largest pocket of labeled water (120 m) resulted in the shortest traveltime, and the model with the smallest pocket (30 m) resulted in the largest traveltime, Fig. 8. An interesting finding is that proximity sensing appears to be sensitive to features that are comparable to the wavelength of the signal. A 30 m pocket of labeled water, which is roughly twice as big

Fig. 6 Received transients for the waterflood models. The results show that proximity sensing is sensitive to moving fronts of labeled brine. An unexpectedly high signal attenuation is observed for models with labeled brine.

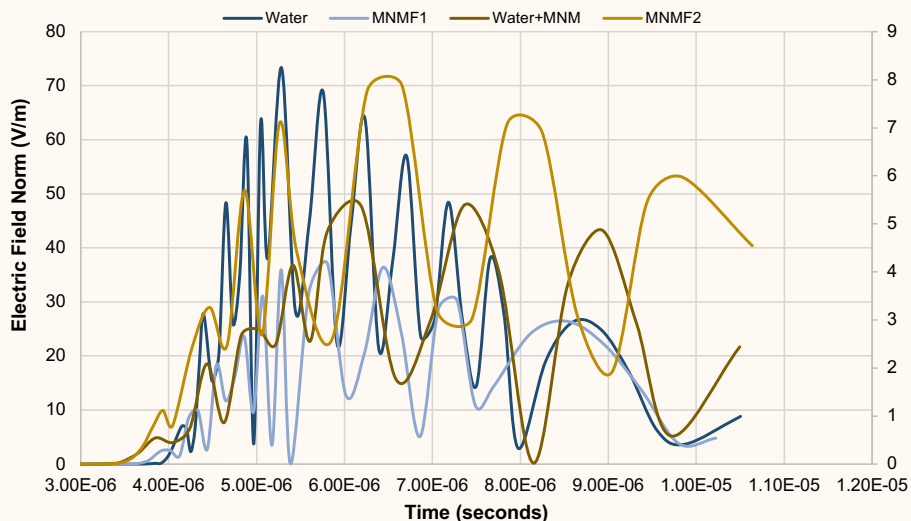
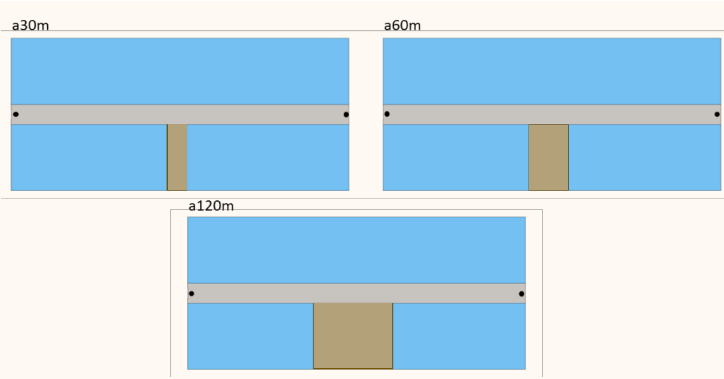


Fig. 7 Models used to evaluate the sensitivity of proximity sensing to isolated pockets of labeled brine. The sections colored in blue represent a brine saturated reservoir; the sections colored in gold represent a reservoir saturated with labeled brine. The axis of symmetry is along the left edge of the models.



as the wavelength, has a significant effect on the signal traveltime. Subsequently, this result is not surprising given that the maximum resolution of this method is expected to be approximately one-quarter of the wavelength. As in the results previously discussed, the addition of the m contrast agents significantly reduces the signal amplitude. While this is unexpected, it has been a consistent trend in the results presented.

Conclusions

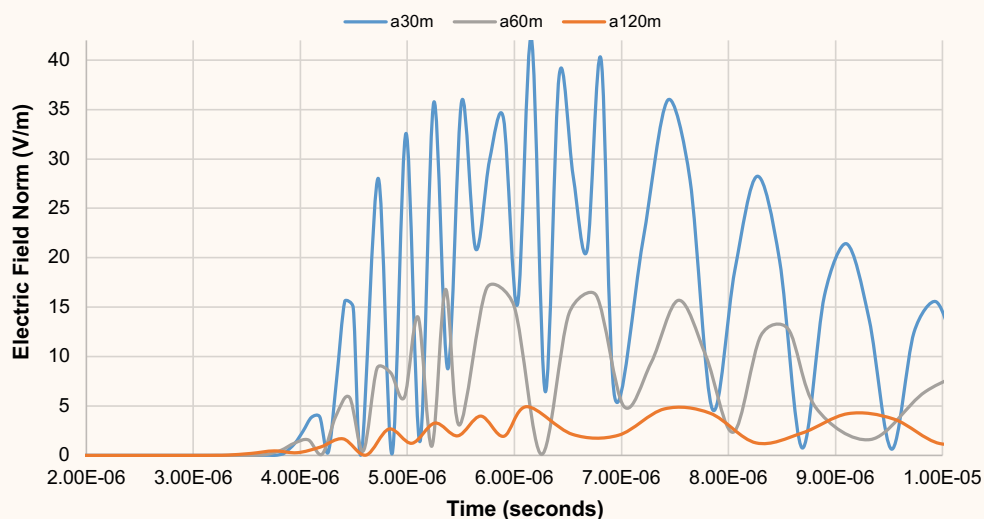
Previous research suggested that proximity sensing is an effective approach to provide saturation information at increased ranges and improved resolution. So far, it had been proposed that this technique could be used to

differentiate between water-saturated and oil-saturated regions of the reservoir based on the ϵ contrasts, making it a suitable method to survey reservoir saturation. The results presented in this work suggest that proximity sensing can also be used in combination with magnetic nanomappers and other contrast agents to map waterflood front movement in the reservoir based on the m contrasts. This approach seems to be effective at detecting continuous fronts and isolated pockets of magnetically labeled water. This means that for flood front mapping purposes, contrast agents can be injected in the form of slugs instead of being continuously injected.

The results show the expected trend for traveltime, and that by increasing the m of the bounding reservoirs, it results in a shorter traveltime, similar to what was previously reported for the ϵ . Consequently, changes in the m seem to have an unexpected effect on signal amplitude. While previous simulations and laboratory experiments reported that increasing the ϵ of the bounding layers increases signal amplitude as a result of energy confinement within the resistive channel, increasing the m results in decreased amplitude. Further simulations and experiments are required to confirm this behavior and investigate the cause.

Using 2D axisymmetric models limits our ability to investigate alternative antenna polarizations. Previous simulations and experiments reported that for the ϵ contrasts, antenna polarization has a significant effect on traveltime. While all the simulations presented in this work were done using vertical electric field polarization, experimental work suggests that for the ϵ changes, greater sensitivity may be achieved using horizontal electric field polarization. It would be informative to evaluate the effect of polarization on the sensitivity of this approach

Fig. 8 Received transients for the models used to evaluate the effect of isolated pockets of labeled brine on traveltime. The results show that adding pockets of labeled brine reduces traveltime. The reduction is directly related to the pocket size.



to map the μ changes.

The results suggest that proximity sensing can be used not only to map oil saturation, but also to monitor injected water movement in the reservoir. When deployed, this approach has the potential to provide reservoir fluid saturation and movement at greatly increased ranges and resolutions. Laboratory experiments will be conducted in the future to validate the simulation results and provide quantitative information about the range and resolution.

Acknowledgments

The author would like to thank the management of Saudi Aramco for their support and permission to publish this article.

This article was presented at the SPE Asia Pacific Oil & Gas Conference and Exhibition, Brisbane, Australia, October 23-25, 2018.

References

1. Pathak, R.K. and Bakar, R.: "Estimating Saturation Changes from 4D Seismic: A Case Study from Malay Basin," IPTC Abstract 16910, presented at the International Petroleum Technology Conference, Beijing, China, March 26-28, 2013.
2. Tolstukhin, E., Lyngnes, B. and Sudan, H.H.: "Ekofisk 4D Seismic — Seismic History Matching Workflow," SPE paper 154347, presented at the SPE Europec/EAGE Annual Conference, Copenhagen, Denmark, June 4-7, 2012.
3. Kelamis, P.G., Uden, R.C. and Dunderdale, I.: "4D Seismic Aspects of Reservoir Management," OTC paper 8293, presented at the Offshore Technology Conference, Houston, Texas, May 5-8, 1997.
4. Denney, D.: "Saturation Mapping from 4D Seismic Data in the Staffjord Field," *Journal of Petroleum Technology*, Vol. 52, Issue 11, November 2000, pp. 38-40.
5. Marvillet, C., Al-Mehairi, Y.S., Shuaib, M., Al-Shaikh, A., et al.: "Seismic Monitoring Feasibility on Bu-Hasa Field," IPTC paper 11640, presented at the International Petroleum Technology Conference, Dubai, UAE, December 4-6, 2007.
6. Marsala, A.F., Al-Ruwaili, S.B., Sanni, M.L., Shouxiang, M.M., et al.: "Crosswell Electromagnetic Tomography in Haradh Field: Modeling to Measurements," SPE paper 110528, presented at the SPE Annual Technical Conference and Exhibition, Anaheim, California, November 11-14, 2007.
7. Aziz, A.A., Strack, K. and Hanstein, T.: "Surface-to-Borehole TEM for Reservoir Monitoring," SEG paper 2011-1882, presented at the SEG Annual Meeting, San Antonio, Texas, September 18-23, 2011.
8. Marsala, A.F., Buali, M., Al-Ali, Z.A., Shouxiang, M.M., et al.: "First Borehole to Surface Electromagnetic Survey in KSA: Reservoir Mapping and Monitoring at a New Scale," SPE paper 146348, presented at the SPE Annual Technical Conference and Exhibition, Denver, Colorado, October 30-November 2, 2011.
9. Marsala, A.F., Lyngra, S., Widjaja, D.R., Laota, A.S., et al.: "Fluid Distribution Inter-Well Mapping in Multiple Reservoirs by Innovative Borehole to Surface Electromagnetic: Survey Design and Field Acquisition," IPTC paper 17045, presented at the International Petroleum Technology Conference, Beijing, China, March 26-28, 2013.
10. Colombo, D., McNeice, G.W. and Kramer, G.: "Sensitivity Analysis of 3D Surface-Borehole CSEM for a Saudi Arabian Carbonate Reservoir," paper presented at the Society of Exploration Geophysicists Annual Meeting, Las Vegas, Nevada, November 4-9, 2012.
11. Felix Servin, J.M., Schmidt, H.K. and Ellis, E.S.: "Improved Saturation Mapping Using Planar Transmission Lines and Magnetic Agents," SPE paper 181343, presented at the SPE Annual Technical Conference and Exhibition, Dubai, UAE, September, 26-28, 2016.
12. Felix Servin, J.M., Ellis, E.S. and Schmidt, H.K.: "Proximity Sensing: A Novel Approach to Reservoir Saturation Monitoring Using High Frequency Electromagnetic Pulses," SPE paper 187282, presented at the SPE Annual Technical Conference and Exhibition, San Antonio, Texas, October 9-11, 2017.
13. Schmidt, H.K., Felix Servin, J.M., Ellis, E.S.: "Experimental Verification of a New Approach to Long-Range EM Imaging," SPE paper 192333, presented at the SPE Kingdom of Saudi Arabia Annual Technical Conference and Exhibition, Dammam, Saudi Arabia, April 23-26, 2018.
14. Emslie, A.G. and Lagace, R.L.: "Propagation of Low and Medium Frequency Radio Waves in a Coal Seam," *Radio Science*, Vol. 11, Issue 4, April 1976, pp. 253-261.
15. Al-Shehri, A.A., Ellis, E.S., Felix Servin, J.M., Kosynkin, D.V., et al.: "Illuminating the Reservoir: Magnetic NanoMappers," SPE paper 164461, presented at the SPE Middle East Oil and Gas Show and Conference, Manama, Kingdom of Bahrain, March 10-13, 2013.

About the Author

Jesus M. Felix Servin

M.S. in Chemical and Biological Engineering, King Abdullah University of Science and Technology

Jesus M. Felix Servin joined the Reservoir Engineering Technology Division of Saudi Aramco's Exploration and Petroleum Engineering Center – Advanced Research Center (EXPEC ARC) in February 2012. His focus is on the development of electromagnetic methods and nanoparticle-based contrast agents for reservoir characterization and monitoring. Jesus's role has been instrumental in the development and deployment of the Magnetic Nano-Mappers project, including hardware design and in-house fabrication, instrumentation, computer programming, and data

processing.

Jesus' interests include the development of nanoscale strategies for reservoir illumination and electromagnetic methods for reservoir description and monitoring.

He received his B.S. degree in Engineering Physics from Instituto Tecnológico y de Estudios Superiores de Monterrey, Monterrey, Mexico, and an M.S. degree in Chemical and Biological Engineering from King Abdullah University of Science and Technology, Thuwal, Saudi Arabia.

Completion Challenges in Unconventional Resources during the Transition Period

Almaz Sadykov, Syed Muhammad, Nayef I. Al-Mulhim, Pavan Dharwadkar, Dr. Lionel B. Small, Sohrat Baki, and Kenneth M. McClelland

Abstract /

Initial exploratory wells in the unconventional program utilized existing well menus that have traditionally been successful for conventional wells. As the unconventional program matured, intensifying stage count, stage volumes, and greater pump rates, it became apparent that the standard accepted practices would no longer be valid. This article addresses the safety and operational challenges that resulted from utilizing a wellhead isolation tool (WHIT) to stimulate unconventional wells completed with 10 Kpsi wellhead components, and provides lessons learned and internally developed best practices. Without comprehensive maintenance procedures, erosion — within the WHIT and completion hardware at the WHIT's outlet — may develop and propagate. This result would compromise the safety and operational integrity of equipment, potentially culminating in a loss of containment.

Mitigation measures were taken to reduce the metal loss, including: (a) the utilization of the WHIT's high rate bullnose and blast joint application, (b) controlling the pump rate and proppant volume, (c) changes in fracturing fluid type, and (d) the addition of degradable fibers with the proppant laden fluid. The WHIT installation and operational practices were developed to limit the number of the mandrel isolation in the same depth position along the stages. Furthermore, the WHIT was investigated for erosion in its body and valve components by physical measurements. Caliper logs were systematically acquired before and after hydraulic fracture treatment stages to evaluate the areas of erosion below the outlet of the WHIT's mandrel, and measure the tubing's wall thickness loss. Highly accurate radial measurements of the inside diameter (ID) variations provided an understanding of the location and severity of mechanical erosion damage generated during the fracturing operation. A result of these investigations and actions was the development and implementation of a comprehensive maintenance plan and tracking system to chart and document the utilization and erosion trends.

Based on caliper log results, erosion was observed, resulting from a turbulence within the tool, due to rapid change in velocity during flow progression from the tool's small diameter mandrel to a larger ID tubing. The WHIT's structural integrity was evaluated after pumping a certain number of stages while recording the volume of proppant, treating pressures, and fluid utilization. Metal losses up to 27% near the end of the WHIT were revealed in the wells completed with 16 fracturing stages and up to 3 million pounds (MM lb) of proppant at 50 barrels per minute (bpm) maximum average pumping rate. The tubing size was 5½" outer diameter (OD). A 4½" OD tube was observed to be susceptible to substantial erosion and its utilization should be considered only in unique circumstances with comprehensive risk mitigation.

Initial solutions implemented included the use of a blast joint, in conjunction with fiber laden fluid and a WHIT with reciprocating stroke and alternating isolation set points. These resulted in a reduction of the maximum metal losses to 4.9% despite the use of 8.9 MM lb of proppant, and a higher maximum average rate of 67 bpm. A long-term solution that was identified was the utilization of 15 Kpsi lower master valve, tubing spool, and hanger with a 15 Kpsi x 10 Kpsi adapter spool and a 15 Kpsi fracturing tree for stimulation operations. After stimulation operations, the wellhead fracture equipment was replaced by a 10 K production tree.

Introduction

For the past decade, there has been a paradigm shift in the oil and gas industry toward the development of unconventional resources. These resources have by and large necessitated long, horizontal wellbores, and multistage hydraulic fracturing treatments, to produce economically. These stimulation treatments often subject wellhead components and downhole assemblies to the highest pressure and abrasive loads in the life cycle of the well. With the high treating pressures and the rates and concentrations of slurry being injected, the wellhead and completion components need to be fit for purpose, to mitigate the prospect of well failures or blowouts.

Unconventional resources in the Kingdom have been developed to address gas production in the long-term, to

substitute gas for liquid fuels, and to provide potential feedstock for the growing chemical industry¹. Substantial efforts had been made by integrated geosciences and the completion engineering team to move from the exploration to the appraisal phase of the project with future development plans. Unconventional carbonate source rock in the Jafurah Basin proved its production success only with multistage horizontal fracturing and multiple stages. The completion designs of the initial wells during the exploration phase represented a significant challenge due to necessity to utilize the wellhead isolation tool (WHIT) and erosion associated with its utilization. Bartko et al. (2017)² addressed several challenges and limitations that were observed with the initial completion strategy, limiting the increase of the perforation cluster density, the number of stages and proppant volumes per well, and the pumping rates due to erosion of the upper section of the tubing.

Based on the reservoir pressure and expected pressure during production operations, the wellhead pressure rating of 10 Kpsi was typically chosen for Jafurah Basin wells. Since treatment pressures could exceed this pressure rating, a 15 Kpsi WHIT was a cost-effective initial solution to be able to perform the stimulation operations and avoid damaging the wellhead, due to higher pressures resulting from higher rate treatments. Figure 1 shows the WHIT, or tree-saver, which was used to isolate the wellhead from operating pressures that go beyond the designed pressure rating.

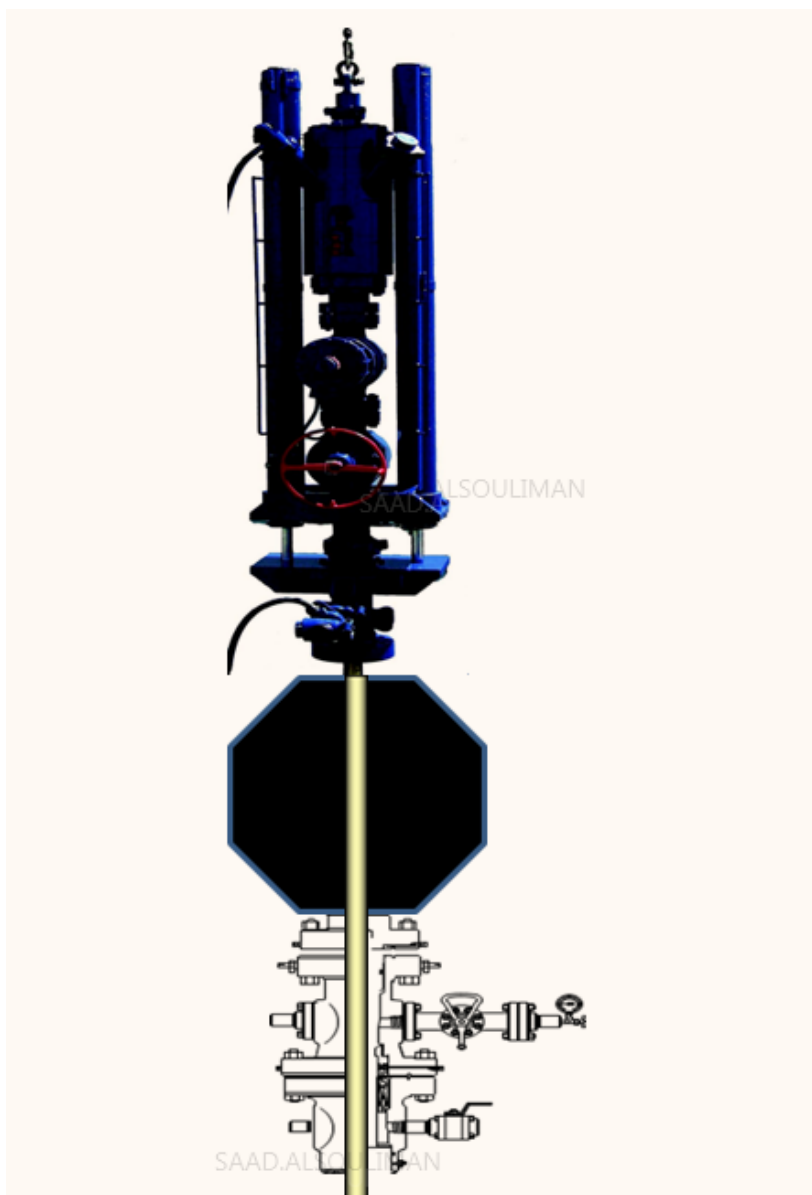
Erosion by abrasive slurries during fracturing treatments in general was previously and frequently addressed in the industry by different studies with some rare references to erosion combined with utilization of the WHIT. Vincent et al. (2004)³ reported about the characteristics of the proppant particles themselves, such as shape/sharpness, mass/density, hardness, and strength, greatly influencing the erosivity of a proppant-laden slurry on well components. They found that ductile materials, such as metal, fail when attacked by abrasives at an angle of less than 45°. In contrast, brittle materials fail at a much higher angle of impingement, and are most severely eroded at a perpendicular angle of attack. Multiple studies have shown that on ductile targets, angular particles — frac sand or resin coated sand — cause significantly more erosion than spherical particles — lightweight ceramics.

It was concluded that the selection and quality control of proppants and materials of the completion itself can have a large impact on erosivity in the tubulars. Severe issues in the upper completion have been reported by EnCana later due to hydraulic fracturing operations in the Horn River development⁴. Computational fluid dynamic modeling confirmed that rotational flow at the inlet mixing point (or the frac tree) can continue down into the first casing connection, and lead to severe erosion near the surface coupled with the actual measured values. Other factors mentioned as being related to such erosion by particle laden slurries, in conjunction with fluid dynamics and flow paths, included the material properties of the pipe, viscosity and density of the carrying fluid, flow type — single or multiphase — and the size,

concentration, and velocity of the particles.

Dimensional changes are experienced by fracturing fluids as they transition out of a WHIT mandrel and into the well tubing, where effects of turbulent flow dynamics and abrasive slurry pumping could combine to cause significant erosion. At this critical juncture, erosion damage can range from nonexistent to catastrophic. This damage can in effect cause the WHIT to itself become a threat to well tubing integrity. Surjaatmadja and Ripley (1992)⁵ found that the type of mandrel used at the end of the WHIT is a critical aspect of the proper WHIT design, and must take into account the flow downstream of the mandrel exit. They mentioned the construction of a WHIT, necessitating to have all parts of the mandrel, including sealing elements, small enough to

Fig. 1 WHIT.



pass all wellhead equipment elements, yet large enough to seal in the tubing. It is one of the main reasons that the internal flow area of a WHIT is typically less, and approximately one-third that of the tubing.

Therefore, as kinetic energy is linearly related to the square of fluid velocity, more than 90% of that kinetic energy is focused in the area directly below the effluence of the WHIT's mandrel, identified as the discharge zone. The flow rate through the mandrel, concentration and the type of proppant, and fluids used were also identified as important parameters in the erosivity of tubulars below the WHIT. The interface design of the mandrel tip, or guide mandrel, WHIT nozzle, or WHIT diffuser, was confirmed to be a crucial component that can govern the effectiveness of the tool in minimizing erosion. Less erosion tendency resulted in the cases where the tip of the mandrel was designed to dissipate kinetic energy within the mandrel parts, without being expended on the tubing wall, i.e., in so-called diffuser type mandrels.

Problem Statement

Any erosion occurring within the tubulars should be considered as a damage and potential threat to well integrity, which could result in potential catastrophic failure. Failure of the WHIT itself during operation could lead to a well control situation where the WHIT's valves are the only barriers.

Therefore, severe erosion weakening design characteristics of completion elements represents a potential for loss of integrity and endangers the safety and environment. Tubing damage could result in expensive repairs and impact economics of any project. Therefore, an understanding of this damage type, location, severity, and the root causes for its occurrence is important for prevention and elimination of such a risk to barrier elements.

In the Jafurah Basin, the effect of erosion on upper completions has been variable. Upscaling completion

parameters necessitated increased proppant volumes with an increasing number of the stages and perforation clusters per stage. Initial wells were completed with 20 pounds per feet (lb/ft) 5½" VM-95HCS and 15.1 lb/ft 4½" Q-125 tubings with the upper section consisting of a corresponding tubing hanger with a short double pin sub. Historically, the WHIT, with an aggressive bullnose design, and a high exit angle nozzle with single staging, was utilized as per conventional low stage count practices until severe erosion was observed in Well-C. This case was investigated and identified with a multifinger imaging tool (MIT) run, which is a multi-caliper logging tool that is used to investigate the integrity of the wellbore.

The erosion found was a result of the discharge zone that is caused by the difference in the internal diameter (ID) of the stinger mandrel with a 2¾" ID and the 5½" 20 lb/ft VM-95 HCS tubing with a 4.778" ID, Fig. 2. The area most susceptible to erosion and potential failure was identified as the first tubing joint and toward the bottom of the double pin sub, mainly due to available stroke length of the WHIT. Erosion took place within a 1 ft interval below where the WHIT's bullnose ends.

Different wall loss scenarios were simulated with tubular design analysis software (WellCat™). Analysis confirmed that wall loss above 30% could represent a heightened risk of tubing failure under the highest operational load parameters. Prior to the wall loss cases, analysis of 20 lb/ft 5½" VM-95 HCS tubing showed the stimulation treatments well within the safe operating limits. Simulating a reduction in wall thickness in the WellCat software, showed that it puts the tubing at the edge of the safe operating envelope during the worst burst case scenario, with a maximum differential pressure of 7,000 psi, expected during the operations, Fig. 3.

Caliper runs were added to completion programs due to the risk of tubing failure and to understand and mitigate the impact of abrasive slurries on completion. This measure was necessary to optimize completion

Fig. 2 The difference in velocities of mandrel discharge zone and tubing where erosion occurred.

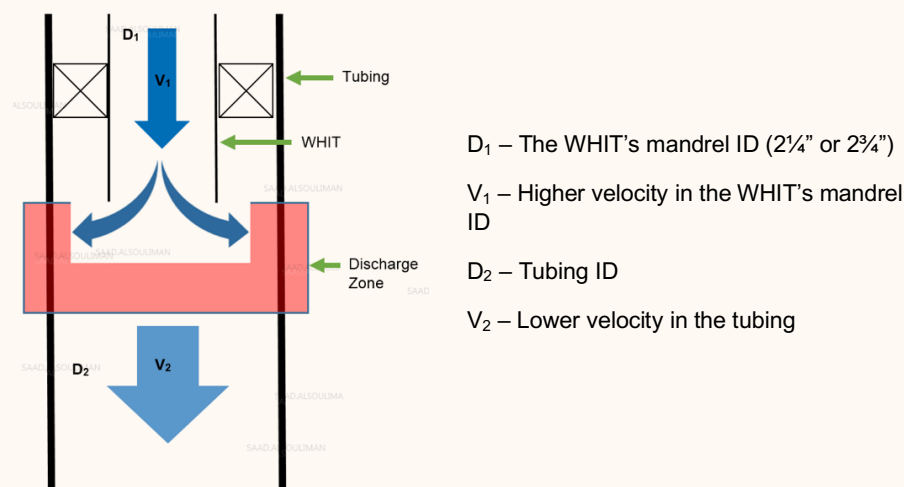
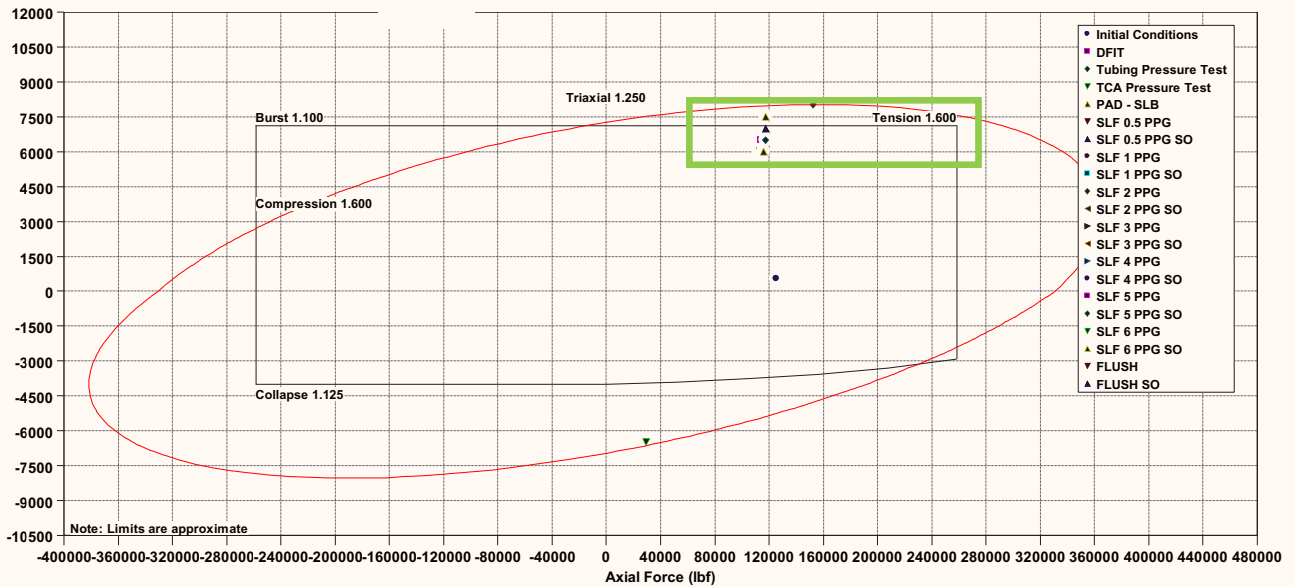


Fig. 3 WellCat™ design limits simulation of 20 lb/ft 5½” VM-95 HCS tubing to model wall loss.



size, which proved to have significant impact on the productivity of the wells. Erosion occurred in many wells due to stimulation and was confirmed by running the MIT logs.

Changing the fluid system to a lower viscosity fluid with higher rates increased abrasion, which resulted in severe erosion within the WHIT itself. The WHIT integrity inspection, with increased amounts of proppant, also had to be addressed for mitigation of any potential erosion.

Short-Term Solutions for WHIT Erosion Mitigation

Well-C was one of the initial wells completed with 13 stages and 3.5 million pounds (MM lb) of high strength proppant (HSP) pumped at an average maximum rate of 60 barrels per minute (bpm), with proppant concentrations ranging from 0.25 to 6 pounds per gallon added (PPA). After the severe erosion of 20 lb/ft 5½” VM-95 HCS tubing was observed in this well, several solutions were proposed and conveyed immediately as short-term ones, to mitigate the potential for tubing failure, due to erosion, until completion upgrade implementation.

These included:

- The use of a high rate bullnose with a much less extreme exit angle.
- Controlling pump rate and proppant volume.
- Lengthening the stroke of the WHIT and alternating positions throughout the treatment, so that the same area of tubing is subjected to less erosion in the discharge zone.
- The utilization of a blast joint below the double pin sub to provide a thicker pipe.

To analyze and quantify the extent of damage to the tubing due to erosion, the MIT was used. The MIT consists of 40 calipers deployed as hard surfaced fingers to accurately measure the internal dimensions along the pipe wall, Fig. 4. With expected, and observed, erosion near the tubing hanger hardware, the MIT was run within the first 200 ft of the wellbore. The radial measurements of the ID of the tubing was processed and an estimated amount of erosion, or wall loss, was provided. MIT analyses were run as baseline, mid-stage, latter stage, and at the final stage, depending on the

Fig. 4 An example of the MIT.

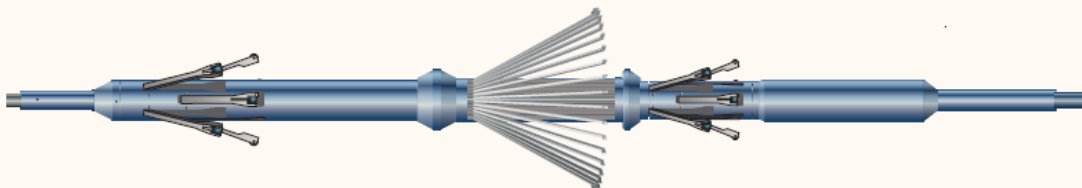


Fig. 5 Well-B MIT results after completion of all stages.

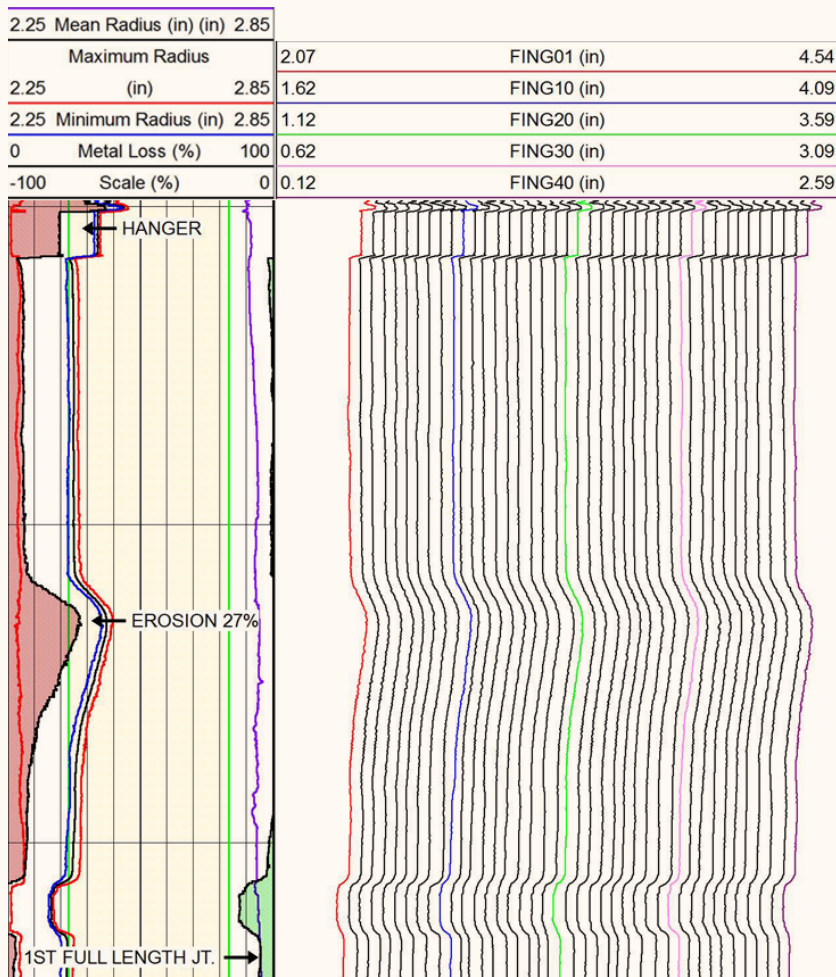
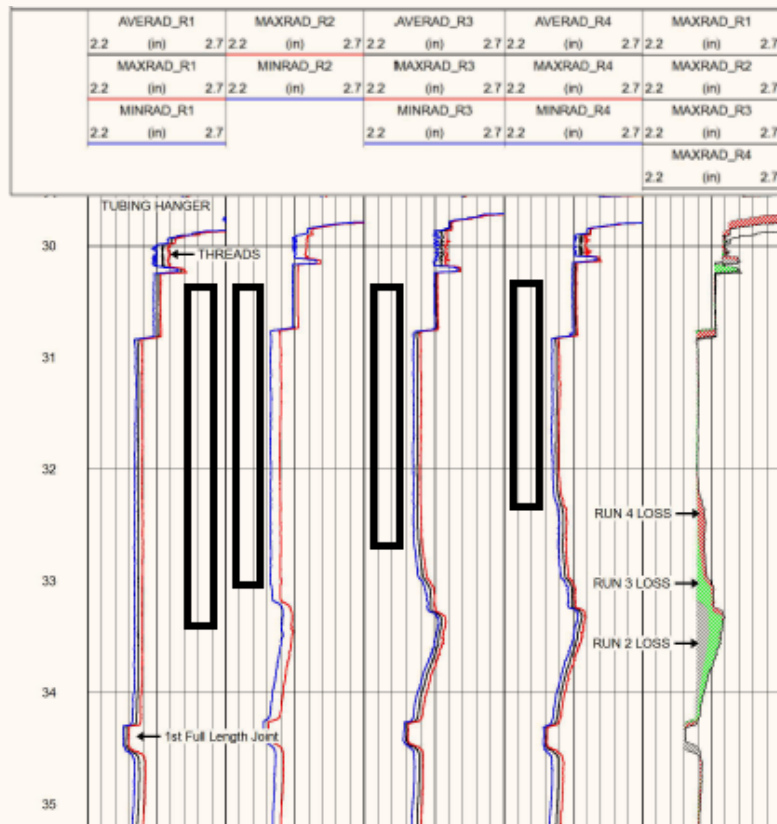


Table 1 Key wells' completion parameters and caliper runs showing maximum wall loss.

Well Name	Total Proppant (MM lb)	Stage Count	Rate (bpm)	Wall Loss (%)	Comment
Well-B	2.90	16	50	27	The well was logged after Well-C.
Well-C	3.04	13	60	>30	The well had severe erosion.
Well-E	4.20	16	54	28	Alternating positions with aggressive bullnose and introduction of high rate bullnose.
Well-H	3.08	16	60.5	5	Fiber inclusion.
Well-M	3.40	16	62	1.3	Blast joint and fiber application, MIT results from mid-stage.
Well-S	7.15	20	62	6	Fiber inclusion, high rate bullnose, WHIT staging, MIT results from latter stage.
Well-T	4.03	20	67.2	27	Low viscosity fluids utilization.
Well-U	8.90	20	63	4.9	Fiber inclusion, high rate bullnose, WHIT staging, blast joint.
Well-V	10.02	24	63.7	7.4	Fiber inclusion, high rate bullnose, WHIT staging.

Fig. 6 Well-E time-lapse analysis with different positions of the bullnose.



individual well completion program. Identification of components such as tubing hangers, collars, and pup joints verified the accuracy of the outputs from the MIT runs and the identification of tubing erosion and wall loss. These erosion parameters were correlated to the amount of proppant — abrasive slurry — volumes pumped to predict erosion for subsequent wells, and to develop an alternating positions strategy, to distribute erosion rather than it be in the same spot for all the stages.

As the internal radius increase was identified by the MIT in Well-C, previously completed Well-B was logged and had similar erosion within the 3.95 ft double pin sub, likely due to maintaining a single WHIT position and an aggressive bullnose, Fig. 5. Such erosion was a result of pumping 16 stages with cross-linked fracturing fluid and 2.9 MM lb of proppant at an average rate of 45 bpm with proppant concentrations ranging from 0 PPA to 6 PPA, where some stages had fiber inclusion.

To understand the erosion pattern as a function of proppant pumped, and the position of the mandrel in the well, it was considered to have several MIT runs in the initial wells after specific proppant volumes were pumped, mainly related to the number of the stages in the same position. Table 1 provides the list of key wells where the MIT was allowed to evaluate implementation of different erosion mitigation techniques. Strict control of

the mandrel positioning was prescribed in well programs.

In Well-E with 20 lb/ft 5½” VM-95 HCS tubing, the following plan was developed for positioning the mandrel and WHIT’s exit with several MIT runs, which allowed us to perform time-lapse analysis, Fig. 6:

- A baseline MIT was run to establish initial internal profile (R1).
- The bullnose for the first three stages was set 45” below the hanger flange. A total of 708 Klb of proppant across all three stages was pumped with an average maximum rate of 50.3 bpm, and proppant concentrations ranging from 0 PPA to 6 PPA with cross-linked fluid.
- Then mandrel position was moved up to 41” below the hanger flange for stages 4, 5, 6, and 7. Then, 1,093 Klb of proppant was pumped in total across all four stages in this position with an average maximum rate of 58.6 bpm, and proppant concentrations ranging from 0 PPA to 6 PPA with cross-linked fluid.
- The MIT log was run (R2), and measured a maximum 15% reduction in the tubing wall’s thickness. It could be noted that erosion took place within the 1 ft interval below the mandrel exit.
- Then, the WHIT mandrel exit was moved up by another 4” to 34” below the hanger flange for stages

8, 9, 10, 11, and 12. Then, 1,347 Klb of proppant was pumped in total across all five stages in this position, with an average maximum rate of 55.5 bpm, and proppant concentrations ranging from 0 PPA to 6 PPA with cross-linked fluid.

- The MIT log was run (R3), and revealed 28% erosion development. Significant amounts of proppant pumped in this position could explain such erosion, due to the cumulative abrasion effect.
- After that, the WHIT was moved to the highest position of 34" below the hanger flange for remaining stages 13, 14, 15, 16. 1,078 Klb of proppant were pumped in total across all four stages in this position, with an average maximum rate of 53.5 bpm, and proppant concentrations ranging from 0 PPA to 6 PPA with cross-linked fluid.
- The final MIT run (R4), showed insignificant erosion from the last mandrel position without the further decrease of wall thickness in the most eroded interval, which was approximately 1 ft deeper than the position of the WHIT's mandrel exit. Introduction of a high rate bullnose decreased the total erosion in this case.

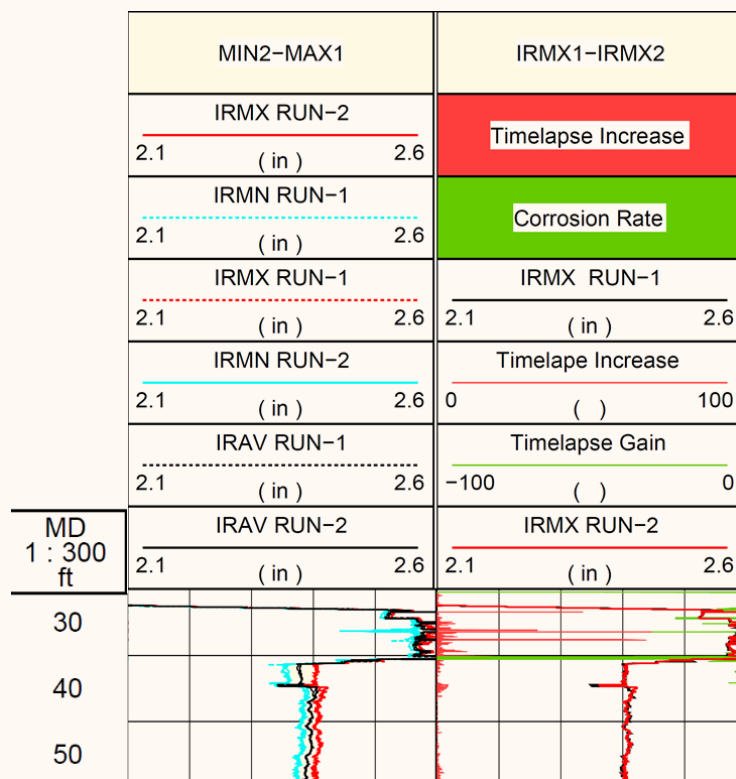
Therefore, implementation of the high rate bullnose and changing its positions in this well allowed us to understand the erosion pattern and distribute it along the upper section of the tubing, to increase proppant pumped in this well without any failure of the tubing.

The total amount of proppant pumped in this well was 4.2 M lb of HSP type, compared to previous Wells B and C with less amounts of proppant. The eroded area sustained high-pressure pumping job pressures, but was not exposed to the worst-case screen out scenario with the maximum differential pressure.

Initial wells were pumped with 3 to 4 MM lb of proppant. Average rates have ranged between 50 bpm to 60 bpm, with rates up to 70 bpm in some stages. Different completion (4½" 15.1 lb/ft Q-125 or 5½" 20 lb/ft VM-95 HCS tubing) showed different erosion results with the similar amounts of proppant and rates applied. MIT runs have confirmed that the 15.1 lb/ft 4½" Q-125 tubing was susceptible to more erosion, as it required a smaller WHIT's mandrel with 2¼" ID, and thereby this increased velocities at the same design rates. The WHIT, during the initial well stimulation, only had an 84" stroke, which limited positions of the mandrel within the upper section of the tubing.

Further improvements in erosion mitigation considered fiber inclusion to cross-linked fluid after the trial test, with the channel fracturing technique in Well-H, which resulted in insignificant erosion during the final MIT run. This log was run after completion of 16 stages with 3.08 MM lb of different proppant types, with an average maximum rate of 60.2 bpm, and proppant concentrations ranging from 0 PPA to 6 PPA, Fig. 7. The maximum wall loss reported was 5%, which was within acceptable range.

Fig. 7 Well-H MIT log time-lapse analysis without erosion pattern after 16 stages.



The utilization of a 5½” 26 lb/ft blast joint with 4.562” ID, or a section of thicker tubing, was also implemented in three wells along with a high rate bullnose and alternating stinger positions. The first well, Well-M with the blast joint, showed negligible (1.3%) erosion after 1.76 M lb of proppant was pumped with an average maximum rate of 59.8 bpm, and proppant concentrations ranging from 0.5 PPA to 6 PPA with cross-linked fluid; a 2¼” ID mandrel was used with the WHIT. Together, with other mitigation measures, particularly in this case with fiber inclusion, it appeared also to reduce impact of the erosion issues. Although it did not find a wide application, due to the introduction of a restricted ID, which could have a potential impact on artificial lift installations in unconventional wells. The smaller ID also limited the pumping rate on the surface to 62 bpm, due to the standard mandrel size with a 2¼” ID. A modified cup tool, only designed for 26 lb/ft 5½” outer diameter (OD) TN-95HS tubing, was later allowed to increase the ID of the mandrel from 2¼” to 2¾” ID, with a subsequent increase of pumping rates within the 65 bpm to 70 bpm range.

Process improvements such as the high rate bullnose, longer WHIT stroke with multiple staging points, and the use of a fiber-laden proppant have decoupled the function of proppant volume on erosion in the upper completion. Limited erosion was always seen in the wells that used these erosion mitigation techniques, depending on completion size. Although fiber had not been primarily considered as an erosion mitigation tool, evidence had shown that it could be preventing a significant amount of erosion in the Jafurah Basin wells.

Concentrations of fiber used were to benefit proppant suspension, and not representative of the minimum fiber concentration that could help to develop laminar flow and prevent erosion at the discharge of the WHIT. Fiber-laden fluid and a WHIT with reciprocating stroke and alternating isolation set points has reduced the metal losses, and facilitated an improvement of fracturing completion parameters with cross-linked fluids, such as pumping rates, proppant, and fluid volumes per well, and increased the number of clusters per stage, while minimizing the amount of erosion to acceptable levels.

For example, Well-S showed only 6% wall loss after stage 15 with a total of 4.9 MM lb of proppant pumped, with an average maximum rate of 60.6 bpm by completion of that stage. An additional five stages were pumped, eliminating the final stage MIT run, due to insignificant expected erosion.

Movement of the mandrel from top to bottom was considered as a preferable way to isolate, by the WHIT’s sealing cups, potentially eroded sections of the tubing, and avoid a cumulative erosion effect. Table 2 shows an example of WHIT staging for one of the wells completed with 20 stages, which was controlled in the well program. Multiple positions were a result of introducing a WHIT with a longer stroke.

Different treatment designs were considered in the Jafurah Basin with low viscosity fluids for increasing stimulated reservoir volume where the candidate well had to use the WHIT. Well-T was the first well to utilize a hybrid treatment consisting of a linear gel followed by cross-linked fluid at the higher PPA stages. This treatment also featured higher pumping rates, averaging around 70 bpm and going up to 80 bpm.

The initial eight stages were pumped per the hybrid design with no fiber in the cross-linked steps. An MIT log was run after these stages and identified erosion of up to 14% wall loss at the egress of the WHIT after 2.1 MM lb of proppant. Stages 9 to 16 were then pumped in the same manner as the first eight, but added fiber at the recommended concentrations to the PPA steps above 1.25. Another MIT log was run and showed wall loss due to erosion of up to 27% after an additional 1.8 MM lb of proppant, approaching levels deemed critical through tubing design simulations and field experiences in the basin. Knowing that fiber-laden fluid was only run for the last one-third of any given stage with cross-linked fluids, it was concluded that leaner fluids pumped with proppant at higher rates caused significant erosion at the discharge of the WHIT. Despite mitigation measures to protect the tubing below the exit of the WHIT, severe erosion was found within the WHIT itself, particularly at the tool’s hydraulic valve.

This finding stopped further treatments with low viscosity fluids via the WHIT until long-term solution

Table 2 Sample WHIT staging chart.

Stage	Depth (below tubing hanger)	Prop Volume
1-3	5”	1.05 MM lb
4-6	11”	1.15 MM lb
7-9	21”	1.35 MM lb
10-12	27”	1.15 MM lb
13-15	33”	1.05 MM lb
16-18	37”	1.35 MM lb
19-20	41”	0.9 MM lb

measures were implemented. The experience gained with cross-linked fluids allowed us to upscale safely and successfully the completion sizes to improve production results. For example, Well-U and Well-V provided the most complete data sets. Well-U had the blast joint in the upper section of 20 lb/ft 5½" OD VM-95HCS tubing and showed only 4.9% erosion despite 24 stages with 8.9 MM lb of proppant, pumped with an average maximum rate of 67 bpm, and proppant concentrations ranging from 0.5 PPA to 6 PPA with fiber-laden cross-linked fluid. Well-V, with a thicker 26 lb/ft 5½" OD TN-95HS tubing, had only 7.4% wall loss after pumping 24 stages with 10 MM lb of proppant, pumped with an average maximum rate of 67 bpm, and similar proppant concentrations with fiber utilization. The pumping rate was limited to 65 bpm to 70 bpm in the design for the 2¾" ID WHIT mandrel. The WHIT mandrel's modified cup tool was required for isolation due to reduced tubing ID in both of these wells.

Examination of proppant types demonstrated that there was no significant difference in erosion based on whether HSP or intermediate strength proppant was being run, and it was mainly related to mitigation measures implemented. The type of fluid in Well-T was found to be an important parameter in the significance of erosion in the tubular, mainly due to the combination of low viscosity fluid, necessitating utilization of higher rates for proppant transport and placement, Fig. 8.

To establish a safe wear exposure limit for the WHIT with an increase in proppant volumes, 2¾" ID WHIT detailed pre- and post-job measurements were performed for all WHITs used in unconventional operations. Measurements included ID measurements before use and after stripping down the WHIT. The ID was measured for all erosion exposed internal wear areas of the WHIT:

sleeves in buffalo head frac ports, hydraulic gate valve, manual gate valve, buffalo head X-over, upper body sleeve, conical sleeve, and mandrel.

The stage count per WHITs inspected ranged from one stage to a maximum of eight stages, from 150,000 lb to 2.8 MM lb proppant exposure. All stages were pumped with cross-linked fluids and at pump rates of approximately 60 bpm with combinations of different proppant types and mesh sizes.

The following conclusions were drawn from an investigation of the WHIT components for erosion, Fig. 9:

1. Up to an exposure of 2.8 MM lb of proppant in cross-linked fluids at 60 bpm, there was no significant erosion wear to the internal components of the WHIT. There was no apparent correlation between exposure and ID change — erosion after 2.8 MM lb was not higher than after 1,000 lb; initial (early) erosion was believed to be caused due to a "run-in effect," where small ID differences between adjacent sleeves were polished away, after that the erosion rate was minimal.
2. Erosion observed during inspections was uniform; spot wear had been observed in one instance (data set 7). Test of the sleeve showed a surface hardness of 52 HRC — lower than an expected hardness of 55 to 60 HRC.
3. The ID wear for two of the early tool inspections (data sets 3 and 4) was found (potentially) outside the hardened zone; overall measurement variations at the start of the project were higher than during the later stage. The initial higher variations were mainly combined with measurement and documentation errors. Data consistency improved once dedicated maintenance personnel performed

Fig. 8 Summary of erosion monitoring results in the Jafurah Basin.

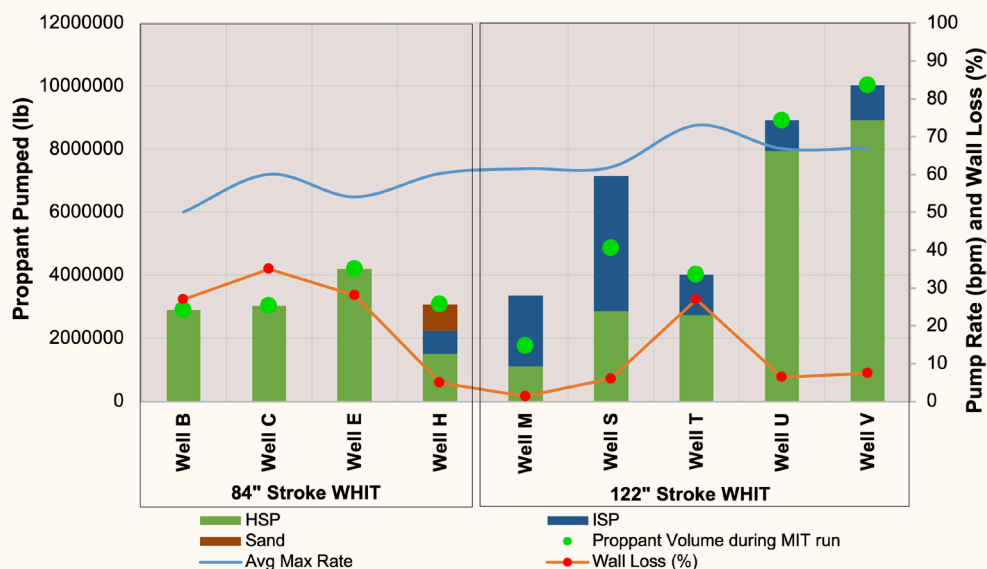
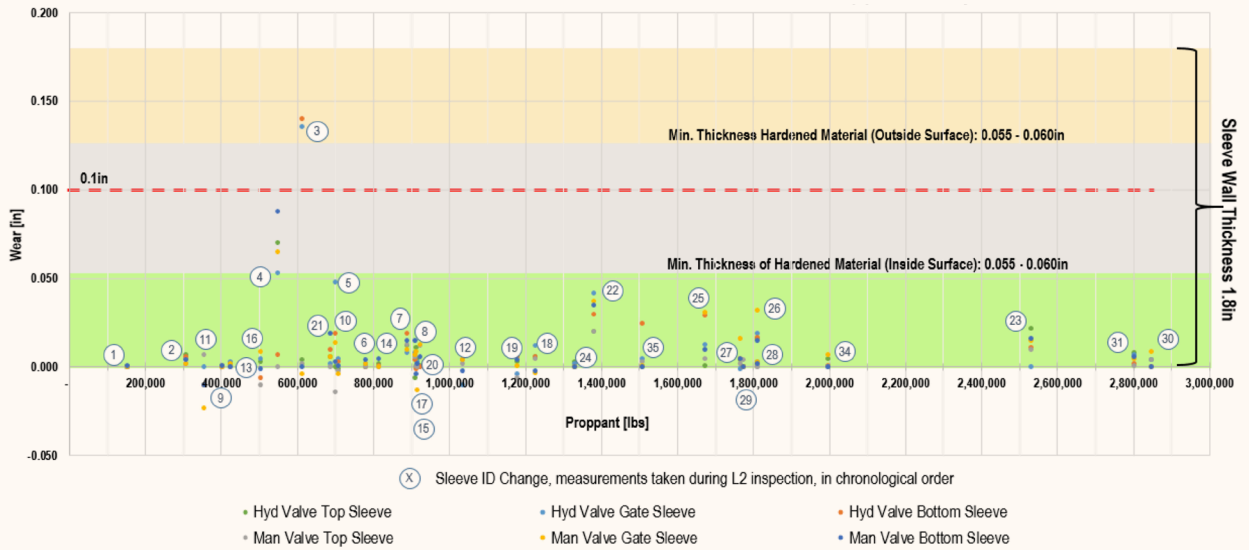


Fig. 9 WHIT valve sleeve wear vs. proppant pumped.



the measurements. Also a more intuitive and logical inspection sheet was developed during the project.

Therefore, the wear sleeve of the WHITs that were exposed — up to 2.8 MM lb of proppant with cross-linked fluids — did not show significant erosion wear. Exposure up to this proppant amount was deemed safe; a further step-wise increase of proppant pumped between tool strip downs was considered to be supported with further measurements. Wear at higher pump rates, or pumping different proppants or low viscosity fluids could not be made due to limitations set in well programs.

As highlighted earlier, findings of severe erosion in the WHIT during operations in Well-T temporarily stopped further applications of low viscosity fluids in the unconventional program until long-term solutions became available. Only cross-linked fluids were considered

together with erosion mitigation techniques as the WHIT erosion pattern with these fluids was negligible, both in the upper tubing section and within the WHIT. Table 3 provides a summary of erosion mitigation techniques with their advantages and disadvantages.

Long-Term Completion Solutions

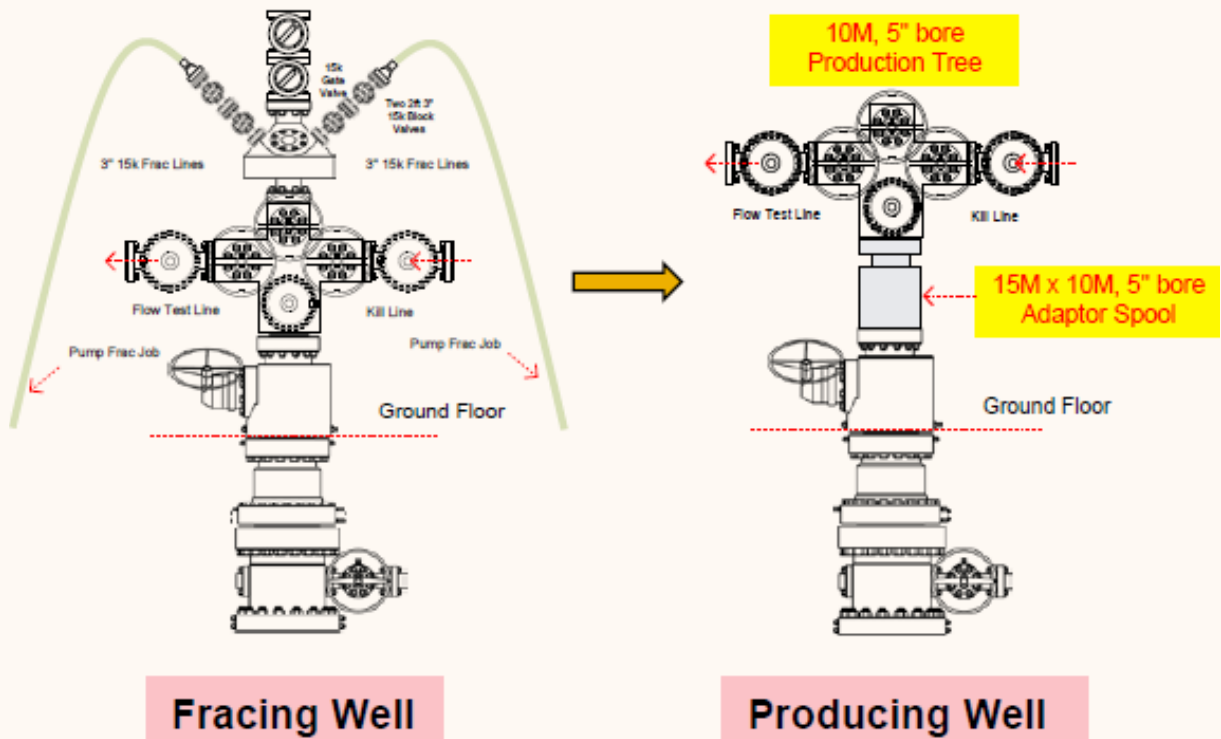
Recommendations from an investigation into the severe erosion observed in Well-C were made early in the unconventional program, to provide a more universal solution to the issue of erosion in the tubulars. These recommendations included a move away from the stopgap measures of WHIT utilization, and the potential restriction of stimulation and artificial lift options, due to the threat of erosion issues.

In an approach to both mitigate risk due to erosion

Table 3 Erosion mitigation techniques summary.

	Erosion Mitigation Technique	Advantages	Disadvantages
1	High rate bullnose	Easy implementation	Cannot fully eliminate erosion
2	Lengthening the stroke of the WHIT and alternating positions	Easy implementation for erosion distribution	Cannot fully eliminate erosion
3	Blast joint inclusion	Thicker wall thickness for erosion	Could represent restricted ID section in upper completion, required modified cup tool for 2.75" ID WHIT's mandrel
4	Fiber inclusion	Substantial erosion limitation, proppant suspension	Additional chemical
5	Controlling treatment rates and fluid type	Easy implementation	Limiting number of clusters per stage to maintain sufficient rate per cluster

Fig. 10 Long-term completion schematic for fracturing and production.



and increase efficiency with the elimination of the rig up/rig down of the WHIT, the use of a 15 K rated lower manual master valve, in conjunction a 15 K rated frac tree was recommended as a long-term solution. The frac tree could then be swapped out with a 10 K production tree using a 15 K x 10 K adaptor spool, Fig. 10.

Completion challenges, combined with WHIT utilization in multistage fracturing, only confirmed that upscaling completion requires these long-term solutions, with complete avoidance of erosion rather than only mitigating it. This was especially true in the case where stimulation treatments transitioned to high rate slick water and hybrid fluid systems. Based on this, special attention should be paid to the integrity of the frac trees and wellhead components themselves, as highlighted by the Well-T experience. Such experience in earlier wells with a WHIT also triggered an investigation of those long-term solutions for any potential erosion issues that could compromise well integrity.

Higher pump rates with 5 $\frac{1}{8}$ " 15 Kpsi frac tree, such as 92 bpm with proppant laden fluid and 100 bpm with clean fluid, allowed further upscaling of the completion and introducing lower viscosity fluids in the Jafurah Basin. Limitation on the frac rate was combined with 60 ft per second of maximum linear velocity of the fluid as an erosional limitation. Similar to the WHIT tearing down frac tree inspections were considered to evaluate erosion after low viscosity fluid treatments. The MIT log was run for evaluation of the upper section and showed absence

of erosion. The post-job back pressure valve setting and retrievals after performing slick water fracturing jobs showed no loss of the profile functionality.

Conclusions

Utilization of a WHIT represented a heightened risk of erosion occurrence in the upper completion and within the WHIT itself with multiple propped fracturing stages, which could only be mitigated. As it represented a safety and financial concern, its use was discontinued.

An analysis of the data collected from the MIT runs on initial wells utilizing a WHIT across the Jafurah Basin led to the following findings with regards to erosion mitigation in an upper completion:

- The 15.1 lb/ft 4 $\frac{1}{2}$ " Q-125 tubing led to significant erosion and wall loss due to a reduced 2 $\frac{1}{4}$ " ID mandrel and significant erosional velocities at 50 bpm to 60 bpm, even with cross-linked fluids.
- Blast joints could provide protection against erosion, but have drawbacks in operational flexibility and artificial lift selection.
- The most preferable solution for the 20 lb/ft 5 $\frac{1}{2}$ " VM-95HC tubing was using in conjunction with a high rate bullnose, fiber laden cross-linked fluid, and 122" WHIT stroke with alternating set points that could mitigate erosion. The maximum pumping rates and proppant amounts were limited to 65 bpm and 1,500 lb accordingly in one WHIT position, and served as a guidance to avoid significant erosion.

- The 26 lb/ft 5½” TN-95HS tubing in the upper completion provided additional protection against erosion, but required the modified cup tool to allow utilization of the 2¾” ID WHIT’s mandrel.
- Hybrid and slick water designs necessitated the use of low viscosity fluids and higher rates could cause the occurrence of significant erosion, not only in the tubing, but also in the WHIT itself. Additionally, the use of higher rates that are required for lower viscosity fluids add to erosion concerns.
- Final MIT runs were only considered after completion of all stages with implementation of erosion mitigation techniques. The MIT runs for the entire vertical section were still recommended for evaluation within the corrosion/erosion monitoring program.

The WHIT components did not show significant erosion of internal elements with limited rates of 65 bpm, and cross-linked fluids after pumping up to 2.8 MM lb of proppant. Risk of erosion was flagged with low viscosity fluids, such as linear gel and slick water at higher rates, 70 bpm to 80 bpm.

Utilization of a 15 Kpsi lower master valve, tubing spool, and hanger with a 15 K x 10 K adapter spool and a 15 K fracturing tree for stimulation operations, which is subsequently replaced by a 10 K production tree, was a successful substitution of the 10 K wellhead component necessitating WHIT utilization. Special consideration still needs to be given to the wellhead components, as rates approach 92 bpm with ceramic proppants, and the utilization of 15,000 psi rated frac trees.

Acknowledgments

The authors would like to thank the management of Saudi Aramco for their support and permission to publish this article. We would also like to thank the teams involved in planning, execution, and evaluation of this project.

This article was presented at the Abu Dhabi International Petroleum Exhibition and Conference, Abu Dhabi, UAE, November 12-15, 2018.

References

1. Al-Mulhim, N.I., Korosa, M., Ahmed, A., Hakami, A., et al.: “Saudi Arabia’s Emerging Unconventional Carbonate Shale Resources: Moving to Horizontals with an Integrated Engineering and Geosciences Approach,” SPE paper 176936, presented at the SPE Asia Pacific Unconventional Resources Conference and Exhibition, Brisbane, Australia, November 9-11, 2015.
2. Bartko, K.M., McClelland, K., Sadykov, A., Baki, S., et al.: “Holistic Approach to Engineered Diversion Aided Completion Providing New Method of Fracture Isolation,” SPE paper 184824, presented at the SPE Hydraulic Fracturing Technology Conference and Exhibition, The Woodlands, Texas, January 24-26, 2017.
3. Vincent, M.C., Miller, H.B., Milton-Taylor, D. and Kaufman, P.B.: “Erosion by Proppant: A Comparison of the Erosivity of Sand and Ceramic Proppants during Slurry Injection and Flow Back of Proppant,” SPE paper 90604, presented at the SPE Annual Technical Conference and Exhibition, Houston, Texas, September 26-29, 2004.
4. Farahani, R., Lastiwka, M., Langer, D., Demirdal, B., et al.: “Assessment and Prediction of Erosion in Completion Systems under Hydraulic Fracturing Operations Using Computational Fluid Dynamics,” SPE paper 147514, presented at the SPE Annual Technical Conference and Exhibition, Denver, Colorado, October 30-November 2, 2011.
5. Surjaatmadja, J.B. and Ripley, H.E.: “Wellhead Isolation Tool Nozzle Design Reduces Erosion of Well Tubing,” *Journal of Canadian Petroleum Technology*, Vol. 31, Issue 10, October 1992, pp. 35-40.

About the Authors

Almaz Sadykov

M.S. in Petroleum Engineering,
Ufa State Petroleum Technological
University

Almaz Sadykov joined Saudi Aramco in 2013 as a Petroleum Engineer in the Unconventional Production Engineering Division, where he worked on rigless activity in the Jafurah, Rub’ al-Khali and South Ghawar areas, with extensive utilization of the plug-and-perf technique for stimulating unconventional gas wells. He currently works in the Technical Support Unit, providing support to stimulation activity in the Jafurah unconventional basin.

Prior to joining Saudi Aramco, Almaz worked for 8 years in stimulation and well production engineering with Schlumberger. He was involved in the design and evaluation of stimulation jobs, completions of oil and gas wells with multistage fracturing systems, and production enhancement.

Almaz received his M.S. degree in Petroleum Engineering from the Ufa State Petroleum Technological University, Ufa, Russia.

Syed Muhammad

B.Eng. in Mechanical Engineering,
University of Aberdeen

Syed Muhammad is a Petroleum (Completion) Engineering Specialist with Saudi Aramco’s Well Completion Operations & Production Engineering Department. He joined Saudi Aramco in 2015, and is currently a part of the Technical Support Unit, providing completion hardware engineering support for all unconventional resources completion

engineering initiatives. Syed has 20 years of experience in completion engineering, having worked extensively in the Asia Pacific, the continental United States, and Alaska, working for both Baker Hughes and ConocoPhillips.

He received his B.Eng. degree (Mechanical) from the University of Aberdeen, Aberdeen, Scotland.

About the Authors

Nayef I. Al Mulhim

*B.S. in Petroleum Engineering,
King Fahd University of Petroleum
and Minerals*

Nayef I. Al Mulhim is leading the South Ghawar and Jafurah Production Engineering Units in Saudi Aramco's Unconventional Production Engineering Division. Previously, he worked with the Southern Area Production Engineering Department, gaining extensive experience in oil and gas production. Nayef has completed an intensive 18-month internship program

with Halliburton Energy Services in North America as a Fracture Engineer.

He received his B.S. degree in Petroleum Engineering from King Fahd University of Petroleum and Minerals (KFUPM), Dhahran, Saudi Arabia, and recently earned the Society of Petroleum Engineers (SPE) Petroleum Engineering Certification.

Pavan Dharwadkar

*M.S. in Petroleum Engineering,
Texas A&M University*

Pavan Dharwadkar is a Completions Engineer currently working at the WD Von Gonten Labs. During his time at Saudi Aramco, he was a part of the Unconventional Resources Well Completions and Production Engineering group helping to drive the production of unconventional gas in the Jafurah Basin.

Prior to his work at Saudi Aramco, Pavan was a Production and Stimulation Engineer with Schlumberger in Denver, Colorado.

In 2011, he received his M.S. degree in Petroleum Engineering from Texas A&M University, College Station, TX.

Dr. Lionel "Bryan" Small

*Doctor of Business Administration,
Walden University*

Dr. Lionel "Bryan" Small initially joined Saudi Aramco in 2001 as a Petroleum Engineer, working with the Abqaiq Production Engineering Division in the Southern Area Petroleum Engineering Department (SAPED). He left the company in 2006 while in the role of Senior Engineer. During the time in SAPED, Bryan oversaw the installation of DTS technology, permanent downhole monitoring system installations together with the drilling and production of the first multilateral wells in the Abqaiq Field. Upon his return to the U.S., Bryan worked for Shell International with subsequent roles in deepwater, unconventional, and artificial lift.

He returned to Saudi Aramco in 2015, assuming the role of Supervisor of Jafurah Production Engineering in October 2016. In March 2018, Bryan moved to the

role of Supervisor of Northern Arabia Production Engineering, and the role of Supervisor of the Technical Support Unit (Completions and Artificial Lift) was added in November 2018. During his second period of employment, his focus has been on the delivery of unique completions and stimulation initiatives to improve EUR and reduce costs in the Jafurah asset, and the successful delivery of the first commercial production from a North Arabia asset.

Bryan received his B.S. degree and M.S. degree in Petroleum Engineering from the University of West Indies, St. Augustine, Trinidad. He received his doctorate in Business Administration (DBA) from Walden University, Minneapolis, MN.

Sohrat Baki

*B.S. in Petroleum Engineering,
Istanbul Technical University*

Sohrat Baki joined Saudi Aramco in December 2013 as a Petroleum Engineer working in the Unconventional Well Completion Operations Department and Unconventional Production Engineering Division. He started his professional career in 2004 with Schlumberger Oilfield Services as a Stimulation Field Engineer in Western Siberia, Russia. Sohrat spent 6 years with Schlumberger in Russia, the North Sea and Europe, where he held additional DESC and Technical Support Engineer positions. Sohrat later spent 3 years with two service companies in the North Sea and

Turkey, where he gained further experience in unconventional resources stimulation, production and project management.

Sohrat's upstream expertise covers production engineering, fracturing, wireline, coiled tubing and project management in exploration and development phases.

In 2003, he received his B.S. degree in Petroleum Engineering from Istanbul Technical University, Istanbul, Turkey.

Kenneth M. McClelland

*M.S. in Business and Technology,
University of New South Wales*

Kenneth M. McClelland joined Saudi Aramco in 2013. He is currently the Technical Support Unit Supervisor for the Unconventional Production Engineering Division of the Well Completion Operations and Production Engineering Department. Kenneth has 18 years of experience in the oil and gas industry, including working as a Team Leader for Santos, Australia; Senior Completions/Operations Engineer for Occidental of Elk Hills, CA; and in various technical and management roles for Schlumberger in Indonesia,

Saudi Arabia, Australia, Angola, U.K. and the U.S. He also has operational and technical training in fracking, coiled tubing (CT) and CT-related operations, for both oil and gas wells located onshore and offshore.

Kenneth received his B.S. degree (with honors) in Mechanical Engineering from Curtin University, Perth, Western Australia, and his M.S. degree in Business and Technology from the University of New South Wales, Sydney, Australia.

A More Sustainable Approach: Nanofiltered Seawater-based High Temperature Fracturing Fluids

Dr. Leiming Li, Dr. Fakuen F. Chang, and Dr. Rajesh K. Saini

Abstract /

In recent decades, the widespread implementation of horizontal drilling and multistage hydraulic fracturing in unconventional plays has increased the use of freshwater in oil field operations. The formulation of fracturing fluids with non-freshwater sources such as seawater or produced water are attracting more attention, due to the long-term sustainability of non-freshwater use.

Fracturing fluids using seawater are available in the industry. But the compatibility between the composition of local seawater and reservoir brine can add complications in the formation damage consideration. For example, if a seawater rich in sulfate comes in contact with formation brine rich in calcium or barium, severe scale can be expected if the proper precautions are not taken. Treated seawater with nanofiltration to remove sulfate is a good practice to eliminate this problem. This article describes a fracturing fluid formulated by using nanofiltered seawater for high temperature applications at 300 °F to 325 °F. The cross-linked fracturing fluid formulation was optimized in the lab to accommodate the nanofiltered seawater, resulting in satisfactory fluid performance, thereby enabling the fracturing operations to conserve freshwater.

A high temperature cross-linked fracturing fluid system was prepared with the nanofiltered local seawater. The fluid system showed robust stability at high temperatures. For example, the fluid viscosity stayed above 400 centipoise (cP) (at 100 sec⁻¹ shear rate) for 2 hours at 300 °F, with 45 pound per thousand (ppt) of the polymer loading. At 325 °F, the fluid maintained viscosity above 300 cP for 2 hours with 60 ppt of the polymer loading. The nanofiltered seawater-based fluids was found to be compatible with a number of commonly used fluid additives including biocide, surfactant, and clay stabilizer. The fluid system also showed low formation damage and scaling tendencies. In the core flow tests at 300 °F, a regained permeability of greater than 95% was obtained. In the scaling tests without the presence of a scale inhibitor at 300 °F, a traceable (< 0.01 wt%) amount of scale was observed in the mixture of the nanofiltered seawater and high total dissolved solids (TDS) formation brine. Overall, it was found that using the nanofiltered seawater can lead to better fluid stability at elevated temperatures, better fluid cleanup, and reduced downhole scaling tendency.

By careful selection of the fluid components, the nanofiltered seawater-based fluid relieves the burden of needing freshwater for hydraulic fracturing treatment, allowing for a more sustainable approach. This article discusses the technical functions of the key fluid additives used in the fracturing fluid preparation.

Introduction

Demand for water used in hydraulic fracturing is increasing continuously, especially due to the implementation of horizontal drilling and multistage hydraulic fracturing in unconventional plays¹⁻³. Recently, oil field operators are pumping bigger fracturing jobs in terms of fluid volume, proppant amount and number of stages per well. These developments are putting an enormous pressure on the use of freshwater for domestic consumption and agricultural applications. The rising cost, and in some regions unavailability of freshwater, has motivated services and production companies to try to prepare fracturing fluids with less ideal water sources such as produced water and seawater⁴. Technically, it is not too difficult to make cross-linked fracturing fluids for medium-to-low temperature applications using water containing high salt concentrations like produced water or seawater^{5,6}. Subsequently, at high temperatures of 300 °F or more, it is much more challenging to make stable cross-linked fluids formulated directly with untreated salt water due to the damage caused by the high levels of salinity and multivalent ions present in the water. When using seawater to formulate fracturing fluids for applications at high temperatures of 300 °F and above, a number of issues emerge related to the high salinity — mostly sodium chloride (NaCl) — and high hardness (mostly calcium (Ca²⁺), magnesium (Mg²⁺), etc.), and other dissolved solids present in seawater.

The high salinity and hardness of seawater negatively affects the stability and viscosity of the seawater-based fracturing fluids, especially at elevated temperatures⁷⁻⁹. Under downhole conditions when the pumped seawater mixes with formation water containing high salinity and hardness, scales could form to potentially plug the formation, and thereby compromise hydrocarbon productions. Scale inhibitors become ineffective at such high temperatures and salinity. It is due to the high scaling tendency that the seawater should be pre-treated to remove specific ions

that contribute most significantly to the scaling based on the formation water composition. Sulfate is one key ion that needs to be removed when formation water contains high concentrations of divalent ions, such as Ca^{2+} , Mg^{2+} , barium (Ba^{2+}), and strontium (Sr^{2+}).

This article presents a new zirconium (Zr) cross-linked, polysaccharide-based fracturing fluid system that was formulated using the nanofiltered seawater for temperatures of 300 °F and above, with the requirement that the fluid viscosity should be above 300 centipoise (cP) (at 100 sec^{-1} shear rate) for 2 hours at the test temperature.

Experimental

Fluid Preparation

The fracturing fluid was prepared by adding a powder or a slurry form of the base polymer in the nanofiltered seawater in a blender jar while blending. The pH of the fluid during hydration was adjusted to between 6 to 7, with a diluted organic acid. The polymer was hydrated for 15 to 20 minutes at a slow blending speed. When the polymer hydration was complete, other fluid additives, including the gel stabilizer, oxygen scavenger, buffering agent, and crosslinking delay agent were added while maintaining the blending. The Zr crosslinker was added last to crosslink the fluid. The pH of the cross-linked fluid was measured in the end to ensure it falls within the crosslinking range.

Rheology Tests

The rheological properties of the cross-linked fluid was measured using a high-pressure, high temperature (HPHT) rheometer equipped with a B5 bob and under 400 psi of nitrogen pressure. The viscosity was measured at 100 sec^{-1} shear rate while raising the fluid to the target temperature, following the API RP 39 schedule. The API RP 39 schedule consists of continuous fluid shearing at 100 sec^{-1} shear rate and a series of shearing ramps at 100, 75, 50, 25, 50, 75, and 100 sec^{-1} once the fluid temperature is within 5 °F of the test temperature, and occurring periodically at every 30 minute interval.

Breaking Tests

Breaking tests were carried out to ensure the proper breakdown of the fluid after hydraulic fracturing treatment and proppant placement. An oxidative breaker was used in the form of a live breaker for breakdown of fluid in the HPHT test. The breaker was added to the fluid just before the addition of the Zr cross-linked to the fluid in the blender. The fluid was then transferred to the rheometer cup, and fluid viscosity was measured following the API RP 39 schedule.

Core Flow Tests

The Parker sandstone core was used to perform the core flow test. The core sample was loaded in a core holder and a confining pressure of 2,500 psi and back pressure of 1,000 psi was applied in the coreflood apparatus, while maintaining the test temperature of 300 °F. In the beginning, 2% potassium chloride (KCl) in a water solution was flown at a rate of 1.0 ml/min through the core sample until the differential pressure stabilized. The permeability of the core was measured with 2% KCl solution at a flow rate of 0.5 ml/min, 1.0 ml/min, 1.5

ml/min, and finally, at 2.0 ml/min along the injection direction.

After finding the permeability of the core sample, the broken cross-linked fracturing fluid was prepared by using: nanofiltered seawater, gelling agent, hydration aid, biocide, clay stabilizer, flow back aid, gel stabilizer, buffer, high temperature stabilizer, Zr crosslinker, and breaker. The fluid was injected in the core at a differential pressure of 500 psi for 30 minutes while maintaining the temperature at 300 °F. The injected fluid was then shut-in overnight for 16 hours at 300 °F. To measure the regained permeability, a 2% KCl solution was injected in the core along the production direction at 1.0 ml/min until the differential pressure stabilized. Then, the differential pressure was measured at the selected flow rates of 0.5 ml/min, 1.0 ml/min, 1.5 ml/min, and 2.0 ml/min, respectively, to calculate the regained permeability.

Scaling Tests

The scaling tests were performed by mixing 20 vol% of formation water with 80 vol% of nanofiltered seawater with and without the addition of various amounts of scale inhibitor. The solutions were heated to the bottom-hole temperature in an oil bath for 2 weeks. After two weeks, the samples were taken out of the bath, photographed, and cooled down to room temperature. The precipitated scale was filtered on filter paper, dried, and then weighed to calculate the amount of scale generation.

Results and Discussion

Fracturing Fluid Preparation and Rheology

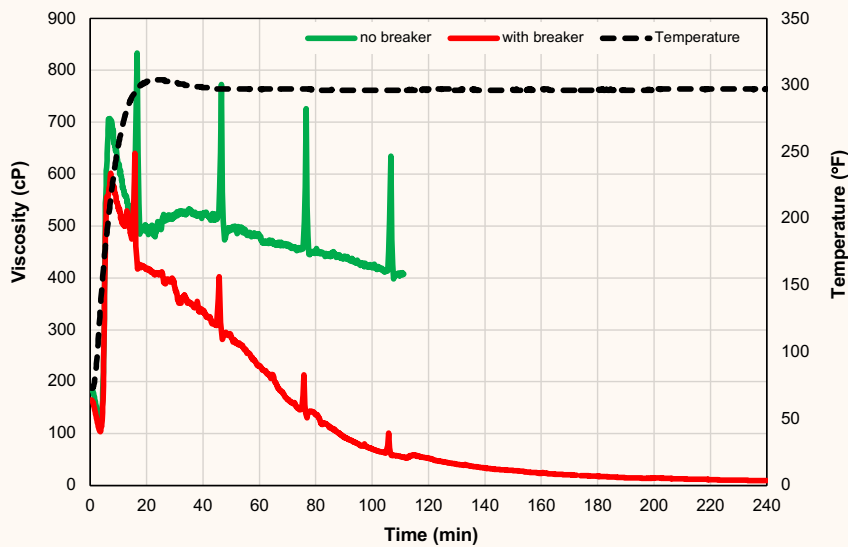
A derivatized guar-based polymer was used as a viscosifying agent for the nanofiltered seawater fracturing fluid. The unfiltered seawater has total dissolved solids (TDS) of around 57,000 mg/L comprising around 2,800 mg/L of multivalent ions, 4,200 mg/L of sulfate ions and rest monovalent ions. The pH of the unfiltered water was around 8.2. Whereas, after nanofiltration, the TDS dropped to around 40,000 mg/L with a substantial reduction of multivalent ions to around 400 mg/L, and the sulfate ions to almost zero. The nanofiltration completely removed the sulfate ions that have the potential to form scale with the formation brine containing divalent and multivalent ions.

The rheology of the nanofiltered seawater-based linear fluid without the crosslinker was measured first at an ambient temperature of 75 °F. The additives in the 45 pound per thousand (ppt) linear gel include a hydration agent, pH increasing buffer, gel stabilizer, high temperature stabilizer, biocide, clay stabilizer, and surfactant. The viscosity profile of linear polysaccharide-based fluids containing additives taken on Fann 35 viscometer (with R1/B1) are listed in Table 1. The n' and K' of the linear fluid at 75 °F was obtained accordingly where $n' = 0.4494$, and $K' = 4.150 \text{ lbf-sec}/100 \text{ ft}^2$.

The baseline cross-linked gel was prepared using a fully hydrated 45 lb linear gel in nanofiltered water containing gel stabilizer, pH increasing buffer, high temperature stabilizer, and Zr crosslinker. The cross-linked fluids were then tested at 300 °F. Figure 1 shows the rheological performance of the baseline cross-linked

Table 1 The viscosity profile of linear polysaccharide-based fluids containing additives.

Speed (rpm)	Shear Rate (s^{-1})	Viscosity (cP)
3	5.1	766
6	10.2	585
100	170	123
200	340	80
300	511	62

Fig. 1 Viscosity profile of the baseline fracturing fluid, without the breaker, and for the fluid with the high temperature oxidizer breaker at 300 °F.

fracturing fluid without the breaker. The fluid pH was 9.2 to 9.3 when measured at room temperature. The fluid viscosity at 300 °F was above 400 cP (at 100 sec^{-1} shear rate) for about 2 hours, exceeding the required fluid specifications — above 300 cP for 2 hours. The related n' and K' values obtained from each of the four ramping peaks are listed in Table 2. These values confirm that the cross-linked fluid is viscoelastic in nature and has shear thinning behavior.

The fluid is designed to crosslink at a higher temperature and is a temperature delayed system. The fluid showed initial viscosity of about 186 cP (at 100 sec^{-1} shear rate) at room temperature. The related linear fluid without the crosslinker had a viscosity of about 170 cP (at 100 sec^{-1} shear rate) at room temperature, suggesting that the crosslinker was not activated at room temperature. The fluid viscosity began to rise quickly when the temperature reached around 120 °F to 130 °F, suggesting that the fluid

Table 2 The n' and K' values of the baseline fracturing fluid (without breaker; in Fig. 1).

Ramping Peak	n'	K' (lbf-sec/100 ft^2)	R^2
1	0.7471	1.9963	0.9408
2	0.7806	1.4527	0.9684
3	0.8021	1.3024	0.9527
4	0.8138	1.1554	0.9486

Fig. 2 Viscosity profile of baseline cross-linked fracturing fluid, without the additives, and for the fluid with three new additives (biocide, clay stabilizer, and flow back enhancing surfactant) at 300 °F. The difference between the viscosities of the two fluids was less than 5%.

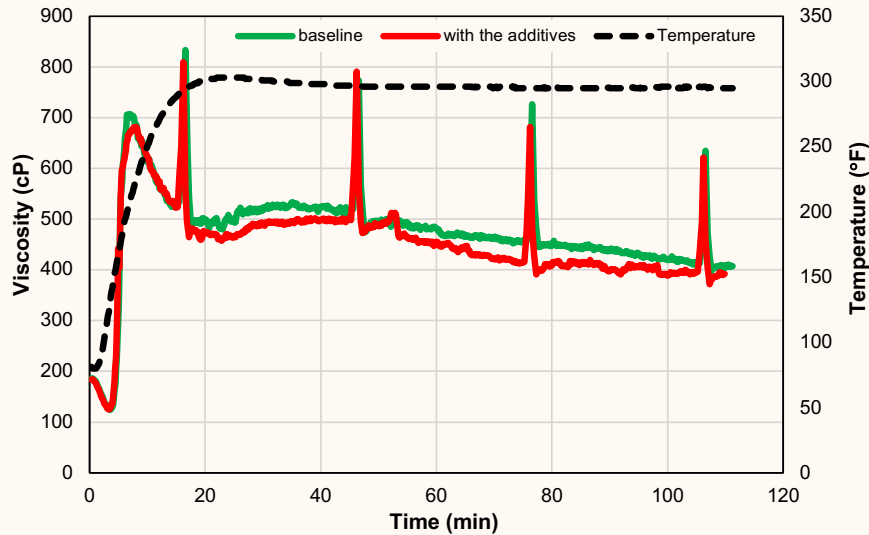
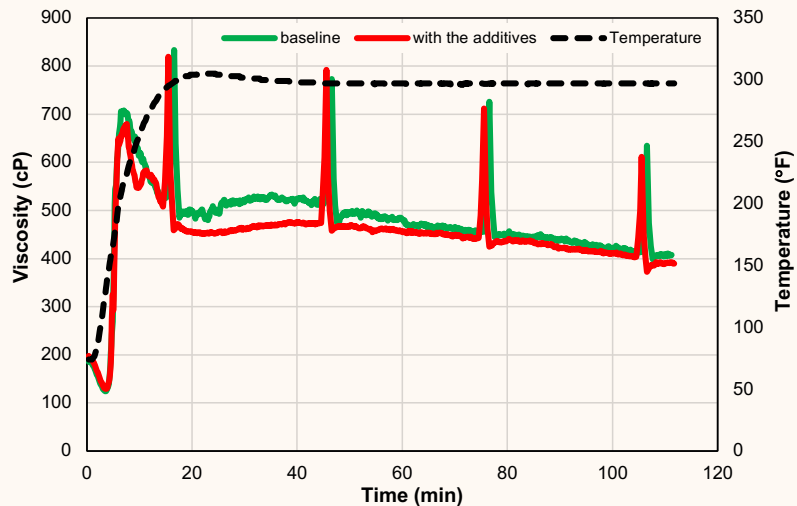


Fig. 3 Viscosity profile of the baseline fracturing fluid, without the additives, and for the fluid with four of the additives (biocide, clay stabilizer, surfactant, and flow back enhancer) at 300 °F. The difference between the average viscosities of the two fluids was less than 6%.



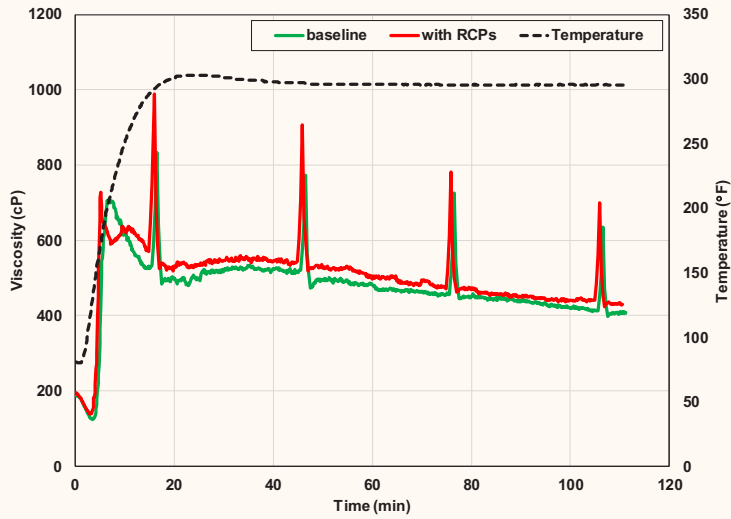
started to crosslink at that temperature. This delayed crosslinking of fluid is advantageous as it prevents the shear degradation during the high-speed pumping through the tubing in a hydraulic fracturing treatment.

When the oxidizer breaker was added to the baseline cross-linked fluid, the viscosity of the fluid at 300 °F decreased faster than the cross-linked fluid without the breaker. The final viscosity dropped below 10 cP in 233 minutes, Fig. 1. The breaking test suggests that the fluid could be sufficiently broken at the test temperature.

Compatibility Tests of Fluid with Additional Additives at 300 °F

The compatibility of the cross-linked fluid prepared with nanofiltered seawater with typical fracturing fluid additives was tested. Figure 2 shows the viscosity profile of the cross-linked fracturing fluid. Biocide, clay stabilizer, and flow back enhancing surfactant are added to the fluid formulation previously described in Fig. 1. The fluid viscosity at 300 °F was again measured. The fluids with and without these three additives are compared and shown in Fig. 2. It can be seen that the additives do not adversely affect the fluid rheology. The viscosity

Fig. 4 Viscosity profile of the baseline fracturing fluid, without the RCP, and fluid with the addition of a mixture of two different 20/40 RCP samples.

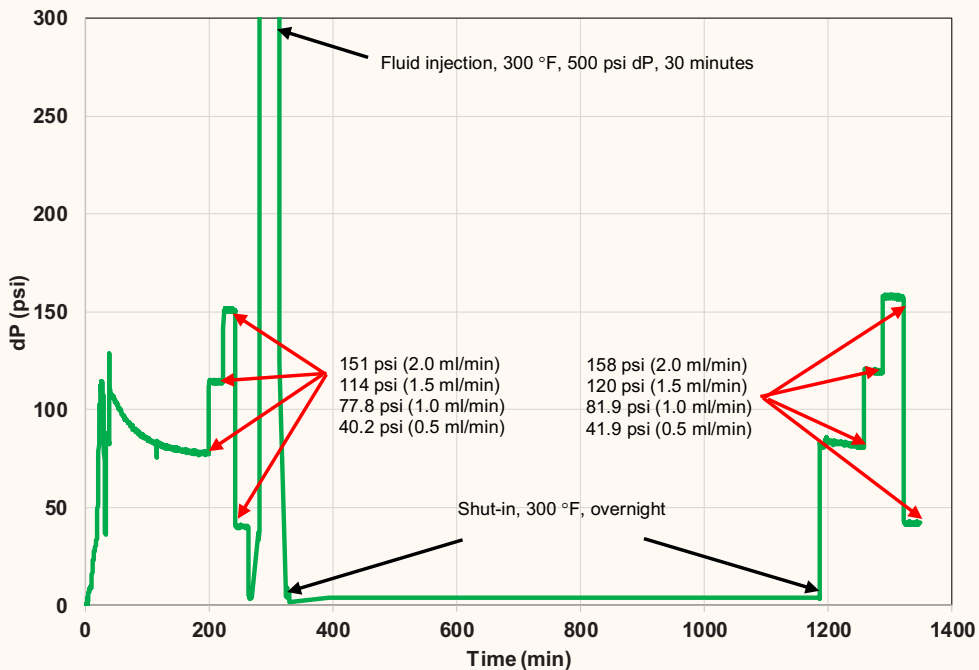


difference between the two fluids was less than 5%, suggesting that the additives were compatible with the cross-linked formulation. The fluid viscosity at 300 °F was still above 300 cP (at 100 sec⁻¹ shear rate) for 2 hours.

In the second set of tests shown in Fig. 3, the baseline fracturing fluid, without the additives, was the same as shown in Fig. 1. This baseline fluid was mixed with four additives, including biocide, clay stabilizer, flow back enhancing surfactant, and a non-ionic surfactant. The

fluid viscosity at 300 °F was measured to be well above 300 cP (at 100 sec⁻¹ shear rate) for about 2 hours. The difference between the average viscosities of the two fluids was less than 6%, suggesting that the four additives were compatible with the fluid formula. Usually, the surfactant and flow back enhancer are not used together in one fluid preparation, and therefore, the compatibility test here could be considered as the “worst-case” scenario as the fluid contained both.

Fig. 5 Plot of change of the differential pressure over time in the core flow test at 300 °F.



The fluid compatibility with the selected resin coated proppant (RCP) was also tested. Figure 4 shows the viscosity profile of the cross-linked baseline fracturing fluid, without the RCP, with the nanofiltered seawater. In the other test shown in Fig. 4, the same baseline fluid was tested with a mixture of two different 20/40 mesh RCP samples at a loading of 0.5 pounds per gallon in the HPHT viscometer. The fluid viscosity at 300 °F was measured to be well above 300 cP (at 100 sec⁻¹ shear rate) for about 2 hours. The two curves nearly traced each other, suggesting that the RCP samples were compatible with the cross-linked fluid. No adverse reduction in fluid viscosity was observed in the test.

Core Flow Test of Nanofiltered Seawater-based High Temperature Fluid at 300 °F

A Parker sandstone core sample was used to perform the core flow test. Confining pressure of 2,500 psi and back pressure of 1,000 psi was applied in the coreflow apparatus, while maintaining the test temperature of 300 °F. In the beginning, a 2% KCl solution was injected at a rate of 1.0 ml/min through the core sample until the differential pressure stabilized. The permeability of the core was measured with a 2% KCl solution at a flow rate of 0.5 ml/min, 1.0 ml/min, 1.5 ml/min, and finally, 2.0 ml/min.

The permeability of the core sample was found to be about 0.77 millidarcies. After the initial permeability measurement, the cross-linked fracturing fluid was prepared with nanofiltered seawater, and contained a gelling agent, hydration aid, biocide, clay stabilizer, flow back aid, gel stabilizer, buffer, high temperature stabilizer, Zr crosslinker, and breaker. The fluid was injected in the core at a differential pressure of 500 psi for 30 minutes while maintaining the temperature at 300 °F. The core was then shut-in for 16 hours at 300 °F. The regained permeability was measured with a 2% KCl solution at 1.0 ml/min until the differential pressure stabilized. Then differential pressure was measured at

the selected flow rates of 0.5 ml/min, 1.0 ml/min, 1.5 ml/min, and 2.0 ml/min, respectively, to calculate the regained permeability.

The average regained permeability achieved was 96%. The relatively high regained permeability value of 96% suggests that the nanofiltered seawater-based fracturing fluid had minimal damage to the core sample at 300 °F. Figure 5 shows the change of the differential pressure vs. time for the core flow test at 300 °F. To have a better view of the leakoff behavior during the fluid injection, the differential pressure vs. the time plot curve was zoomed in from 280 minutes to 310 minutes, Fig. 6. The leakoff effluent volume during the 30 minutes of the fluid injection was also plotted in Fig. 7, and estimated to be about 5.5 ml to 5.7 ml.

Scaling Tests at 300 °F

A scaling test was performed to check if nanofiltered seawater could form scale with formation water under downhole conditions. A mixture of nanofiltered seawater and formation water was used for measuring scaling tendencies. The formation brine contained high TDS of around 300,000 mg/L, with a high concentration of multivalent ions such as 3,800 mg/L of Ba²⁺, 25,000 mg/L of Ca²⁺, 2,000 mg/L of Mg²⁺, 2,000 mg/L of Sr²⁺, and the rest were monovalent ions.

Three samples of a mixture of formation brine and nanofiltered seawater were prepared by mixing 48 ml (80 vol%) of the nanofiltered seawater and 12 ml (20 vol%) of formation brine in the pressure tube. To these tubes added 0 gallons per thousand (gpt) (baseline), 2 gpt, and 4 gpt of scale inhibitor, respectively. The tubes were sealed and placed in the heating bath set at 300 °F. A photograph of each sample tube was taken from time to time. The scaling tests were conducted for 2 weeks.

Figure 8 shows the photograph of the three test samples after two weeks of the scaling tests at 300 °F. A negligible amount of scales were formed in the samples containing 2 gpt and 4 gpt of the scale inhibitor. After the tests,

Fig. 6 Plot of change of the differential pressure from 280 minutes to 310 minutes in the core flow test at 300 °F.

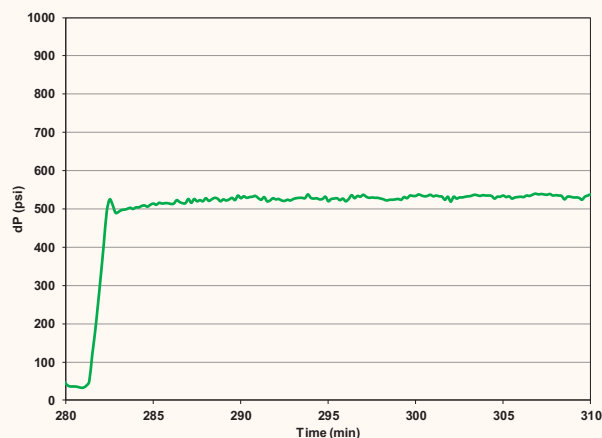
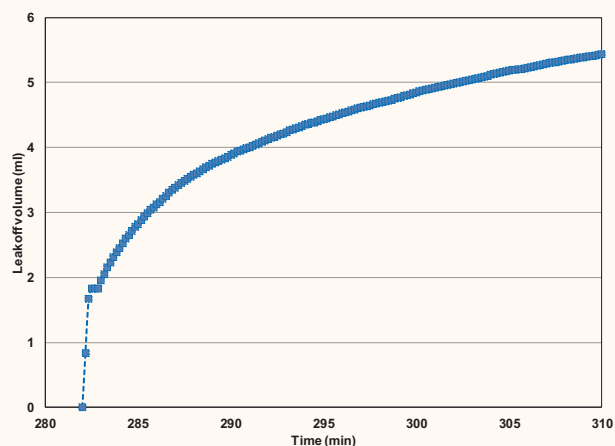


Fig. 7 The leakoff effluent volume vs. time during the fluid injection of the core flow test at 300 °F.



the samples were cooled down to room temperature, filtered, and the weight of the scale (dried) was measured, Table 3. The sample containing 2 gpt and 4 gpt of the scale inhibitor generated no detectable amount of scale. Even without the scale inhibitor, the scale generated was only 0.8 ppt. The significantly reduced scale generation could be explained by the greatly reduced sulfate ion concentration in the nanofiltered seawater.

Fluid Rheology at 325 °F

The nanofiltered seawater-based fracturing fluids were tested at a higher temperature of 325 °F. The fluid formulation was adjusted so that the cross-linked fluid viscosity at 325 °F could be at least be 300 cP (at 100 sec^{-1} shear rate) for 2 hours. After a number of tests, the fluid formulation was optimized to work at 325 °F. A derivatized guar-based polymer at a loading of 60 ppt was used as a viscosifying agent in the nanofiltered seawater

Fig. 8 Scaling tests conducted at 300 °F for two weeks for the mixture of 20 vol% brine and 80 vol% nanofiltered seawater containing the scale inhibitor at dosages of: (a) 0 gpt (baseline), (b) 2 gpt, and (c) 4 gpt.

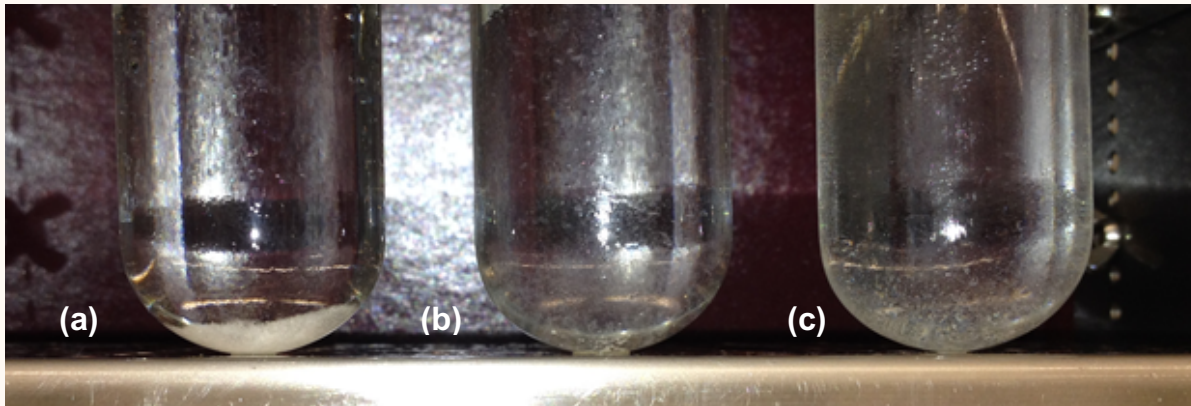


Table 3 Scale generated in the scaling tests

Test	0 gpt	2 gpt	4 gpt
Scale inhibitor added (gpt)	0	2	4
Scales generated (ppt)	0.8	0.0	0.0

Fig. 9 Viscosity profile of the cross-linked fracturing fluid, without breaker, and fluid with live breaker at 325 °F.

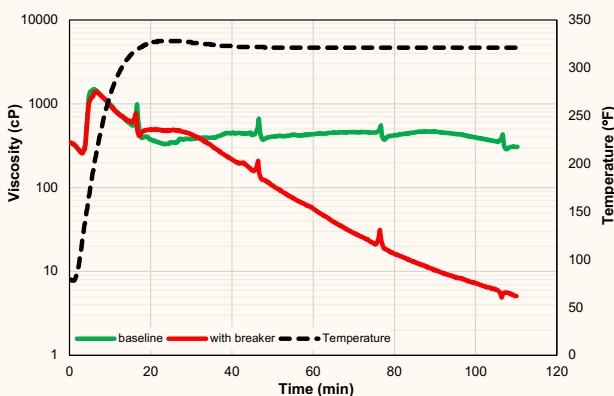
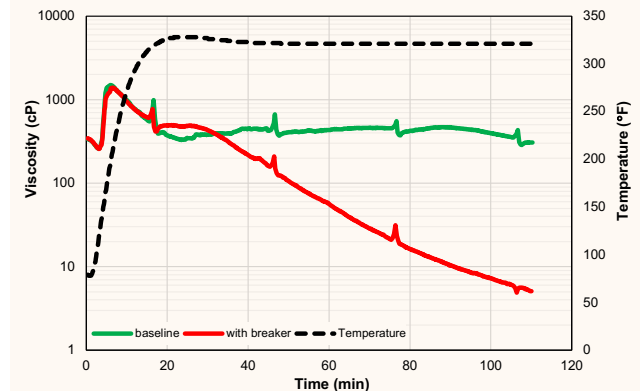


Fig. 10 Viscosity profile of the baseline cross-linked fracturing fluid, without additives, and fluid with three additional additives (biocide, clay stabilizer, and flow back enhancer) at 325 °F and 100 sec^{-1} .



for the base gel. The additive concentration of hydration aid, gel stabilizer, pH raising buffer, high temperature stabilizer, and crosslinker were adjusted accordingly. The fluid pH was 9.6 to 9.7 at room temperature. Figure 9 shows the fluid viscosity at 325 °F, denoted as the baseline, which stayed above 300 cP (at 100 sec⁻¹ shear rate) for about 2 hours. The fluid was designed to crosslink at a higher temperature and is a temperature activated crosslinking system. The fluid showed an initial viscosity of over 300 cP (at 100 sec⁻¹ shear rate) at room temperature. The fluid viscosity began to rise quickly when the temperature reached around 120 °F, suggesting that the fluid started to crosslink at this temperature. The delayed crosslinking of fluid is desirable because it prevents the shear degradation of fluid during the high rate pumping through the tubing.

When a live breaker was added to the cross-linked fluid, the viscosity at 325 °F decreased faster than the fluid with no breaker. The viscosity of fluid with a breaker dropped below 10 cP in about 91 minutes, Fig. 9. The breaking test suggests that the fluid could be sufficiently broken for subsequent flow back of the fracturing fluid.

The compatibility test of the cross-linked fluid was also tested with other fluid additives at a temperature of 325 °F. Figure 10 shows the viscosity profile of the baseline cross-linked fracturing fluid, without additives, prepared using nanofiltered seawater, hydration aid, 60 ppt gelling agent, gel stabilizer, pH increasing buffer, high temperature stabilizer, and Zr crosslinker. The fluid viscosity stayed above 300 cP (at 100 sec⁻¹ shear rate) for about 2 hours at 325 °F. Similarly, in another test as shown in Fig. 10, the baseline fluid was mixed with three additional fluid additives, including biocide, clay stabilizer, and flow back enhancer. Figure 10 also shows that these rheology profiles with additional additives were compatible with the fluid formulation.

Conclusions

1. The nanofiltered seawater-based high temperature Zr cross-linked fluids with polymer loading of 45 lb showed viscosity above 400 cP (at 100 sec⁻¹ shear rate) for about 2 hours at 300 °F. The 60 lb Zr cross-linked fluids showed viscosity above 300 cP (at 100 sec⁻¹ shear rate) for about 2 hours at 325 °F.
2. The nanofiltered seawater-based high temperature Zr cross-linked fluids were compatible with biocide, clay stabilizer, flow back enhancer and an additional surfactant at 300 °F to 325 °F.
3. The cross-linked fluids were also compatible with two RCP samples and did not show any adverse effect on the viscosity.
4. The nanofiltered seawater-based high temperature cross-linked fluid showed greater than 96% regained permeability in the core flow test run at 300 °F.
5. Negligible amounts of scale were generated in the mixture of 20 vol% formation brine with 80 vol% of nanofiltered seawater over 3 weeks of testing at 300 °F.

Acknowledgments

The authors would like to thank the management of Saudi Aramco and Aramco Services Company for their support and permission to publish this article.

This article was presented at the SPE Middle East Oil and Gas Show and Conference, Manama, Kingdom of Bahrain, March 18-21, 2019.

References

1. Economides, M.J. and Nolte, K.G.: *Reservoir Stimulation*, 3rd edition, New York: John Wiley & Sons, 2000, 856 p.
2. Economides, M.J. and Martin, T.: *Modern Fracturing: Enhancing Natural Gas Production*, 1st edition, Houston, Texas: Energy Tribune Publishing Inc., 2007, 509 p.
3. Ajayi, B., Aso, I.I., Terry, Jr., I.J., Walker, K., et al.: "Stimulation Design for Unconventional Resources," *Oilfield Review*, Vol. 25, Issue 2, June 2013, pp. 34-36.
4. Puder, M.G. and Veil, J.A.: "Options, Methods and Costs for Offsite Commercial Disposal of Exploration and Production Wastes," *SPE Projects Facilities & Construction*, Vol. 2, Issue 4, December 2007, pp. 1-5.
5. Li, L., Al-Muntasheri, G.A. and Liang, F.: "Nanomaterials Enhanced High Temperature Fracturing Fluids Prepared with Untreated Seawater," SPE paper 181283, presented at the SPE Annual Technical Conference and Exhibition, Dubai, UAE, September 26-28, 2016.
6. Li, L., Liang, F., Al-Muntasheri, G.A. and Cairns, A.J.: "Hydraulic Fracturing Fluid," U.S. Patent Application No. 20170198207, 2017.
7. Al-Muntasheri, G.A.: "A Critical Review of Hydraulic Fracturing Fluids for Moderate to Ultralow Permeability Formation over the Last Decade," *SPE Production & Operations*, Vol. 29, Issue 4, November 2014, pp. 243-260.
8. Bao, C., Han, J., Li, L., Qiao, C., et al.: "A Stimulation Study on Mitigation of Water Hardness Damages in Fracturing Fluids," SPE paper 178976, presented at the SPE International Conference and Exhibition on Formation Damage Control, Lafayette, Louisiana, February 24-26, 2016.
9. Li, L., Sun, H., Qu, Q., van Le, H., et al.: "High Temperature Fracturing Fluids Prepared with Extremely High TDS and Hard Produced Water," SPE paper 170607, presented at the SPE Annual Technical and Conference and Exhibition, Amsterdam, the Netherlands, October 27-29, 2014.

About the Authors

Dr. Leiming Li

Ph.D. in Materials Science and Engineering, University of Illinois at Urbana-Champaign

Dr. Leiming Li has more than 12 years of experience in the oil and gas industry. His professional interests and achievements are in the development of novel treatment fluids and oil field chemistry solutions. Leiming has developed several new oil field technologies, including for fracturing, high temperature wells, produced water reuse, enhanced oil recovery, sand control and water control, to name a few. He worked as a Senior Lab Scientist at Aramco Services Company for 3 years, Research Scientist at Baker Hughes for 2 years and Support Engineer/Sr. Support Engineer at Schlumberger for 7 years.

Leiming is actively involved in various volunteer services. He serves as the Technical Reviewer for the Society of Petroleum Engineers' (SPE) *Production & Operations*, *SPE Journal*, and the *Colloids and Surfaces A: Physicochemical and Engineering Aspects*. Leiming is also the reviewer for the American Chemical Society Petroleum Research Fund (ACS PRF). He has also published a number of letters in *Chemical & Engineering News* (C&EN) related to the oil field

operations, helping the society to have a better understanding of the petroleum industry. Leiming holds 50 granted U.S. patents, 68 published U.S. patent applications, and has published 42 papers, mainly in SPE conferences and peer-reviewed journals.

He has received several awards at Schlumberger, such as the Performed by Schlumberger Bronze Award in 2009 and 2010 for the development of fluid from produced water and reuse of produced water in oil field applications. In 2011 and 2012, Leiming also received Schlumberger's Innovation Award for three different technologies that he developed. He is also 2018 World Oil Awards finalist for the "Innovative Thinker" category. Leiming is one of the top three inventors by Patentdocs for his invention in the "Earth Boring, Well Treating, and Oil Field Chemistry" category.

He received his B.S. degree in Physics from Tsinghua University, Beijing, China, and a Ph.D. degree in Materials Science and Engineering from the University of Illinois at Urbana-Champaign, Champaign, IL.

Dr. Fakuen "Frank" F. Chang

Ph.D. in Petroleum Engineering, University of Oklahoma

Dr. Fakuen "Frank" F. Chang is the focus area champion for Productivity Enhancement in the Production Technology Team of Saudi Aramco's Exploration and Petroleum Engineering Center – Advanced Research Center (EXPEC ARC).

Prior to joining Saudi Aramco in September 2012, he worked at Schlumberger for 16 years. Before that, Frank was at Stimlab for 4 years. He has developed many products and technologies dealing with sand control, fracturing, acidizing and perforating.

Frank is an inventor and recipient of 23 granted U.S. patents, and he is the author of more than 40 Society of Petroleum Engineers (SPE) technical papers.

Frank received his B.S. degree in Mineral and Petroleum Engineering from the National Cheng Kung University, Tainan City, Taiwan; his M.S. degree in Petroleum Engineering from the University of Louisiana at Lafayette, Lafayette, LA; and his Ph.D. degree in Petroleum Engineering from the University of Oklahoma, Norman, OK.

Dr. Rajesh K. Saini

Ph.D. in Organic Chemistry, Kurukshetra University

Dr. Rajesh K. Saini is a Research Science Specialist in the Production Technology Team at the Aramco Research Center-Houston. He has more than 22 years of experience in the oil and gas industry, and chemical research. Rajesh is a subject matter expert in oil field stimulation, production and operations technology. He specializes in product development, scaling up, intellectual property, sales and commercialization of new products/processes for hydraulic fracturing, sand control, acidizing, production technology, oil field chemicals, and water conformance. Prior to joining Aramco in 2017, Rajesh played critical roles at Halliburton, Weatherford, and Lubrizol in the capacity from Research Scientist to R&D Manager.

He has served as a technical reviewer for major journals, including the *Journal of American Chemical Society*, and the *Journal of Organic Chemistry and Organic Letters*. Rajesh is a Technical Editor for the Society of Petroleum Engineers (SPE) *Production and*

Operations Journal. He is serving on the SPE Annual Technical Conference and Exhibition (ATCE) well stimulation committee. Rajesh holds 54 U.S. patents, 21 U.S. patent applications, and has published one book chapter and 48 peer-reviewed journal articles.

He served as the Distinguish Lecture's Program Chair and Director of the SPE-Southwest Oklahoma Section during 2009-2012. Rajesh received the Maximizing Value-Added Performance (MVP) Award at Halliburton for developing environmental fracturing fluid (CleanStim[®]) and breaker for AquaLinear[®] fluid. In 2018, he was also awarded the SPE Gulf Coast Regional award for Production and Operations.

Rajesh received his MBA from Oklahoma State University, Stillwater, OK, and his Ph.D. degree in Organic Chemistry from Kurukshetra University, Haryana, India. He was a postdoctoral fellow at Rice University working with Prof. W.E. Billups and Richard E. Smalley (Nobel Laureate in Chemistry).

Nanocomposite Resin Coated Proppant for Hydraulic Fracturing

Dr. Mohammad H. Haque, Dr. Rajesh K. Saini, and Dr. Mohammed A. Sayed

Abstract /

Proppant, such as sand and ceramics, is used in keeping fractures open for hydrocarbon production in hydraulic fracturing operations. Its ability to withstand reservoir closure stresses and provide high conductivity is one of its key selection criteria. Sand is preferred over ceramics in unconventional plays due to its low cost and overall abundance. The lower crush strength of sand compared to ceramics limits its application to wells having lower closure stresses. Therefore, it becomes necessary to strengthen the sand as a low-cost solution for demanding downhole conditions. Coating sand with resin is a long-practiced method to strengthen and control fines. One fundamental challenge with resin coated sand (RCS) lies in its overall thermo-chemo-mechanical stability at high-pressure, high temperature in the presence of fracturing fluid.

In this work, a nanocomposite resin has been developed to provide enhanced coating strength and chemical stability. RCS has been characterized from the perspectives of its core and coating. As received sand has been evaluated by: (1) single grain crush testing, (2) optical particle size analysis for sphericity and roundness, (3) X-ray diffraction (XRD) for mineral content and composition, and (4) petrography analysis for microstructure, texture, and crystalline phases. Sand has been coated using phenol formaldehyde (novolac) resin systems reinforced with nanomaterials and altered surface wetting properties demonstrating improved crush strength, chemical resistance and long-term conductivity. Loss on ignition (LOI), American Petroleum Institute (API) proppant crush resistance test, and API long-term proppant conductivity tests have been used to evaluate RCS.

Petrographic evaluation of Northern white (NW) sand shows the presence of plutonic, and monocrystalline grains having a higher crush strength, whereas Texas brown (Brady) sand shows an abundance of polycrystalline and metamorphic grains that are relatively weaker due to impurities, and inner weak planes. The white sands are well sorted and a roundness and sphericity of > 0.6 were measured by optical particle size analysis. With traditional resin coating, the API crush resistance stress of the sand has increased by $\sim 200\%$; whereas, the API long-term proppant conductivity has increased by 41% to 130% compared to uncoated sand. On the other hand, the nanocomposite resin coating containing a combination of nano-reinforcement materials and wettability altering agents has increased the API proppant conductivity by 100% to 244% compared to uncoated sand. Nanomaterial used in the coating contains high surface area nanofibers with an exceptionally high aspect ratio. The synergistic effect of different nanoparticles increased the strength to an even higher level by providing a barrier to the permeation of fluid in the coating, thereby increasing chemical resistance.

An economic and up-scalable nanocomposite coating technology containing a novel combination of nanomaterials and surface wettability altering agents has been developed with improved proppant crush strength, conductivity and chemical resistance. The performance of the coated sand has not been compromised when exposed to fracturing fluid at elevated temperatures, making it a suitable candidate for field applications at higher stresses.

Introduction

The increasing demand of oil and gas is supported through the development of deeper and tighter conventional and unconventional hydrocarbon resources. To achieve economical production rates from such tight formations, the technique of hydraulic fracturing is applied to increase the contact between the reservoir and the wellbore. Two main components are needed in all hydraulic fracturing applications. The first one is the solid particles needed to fill the induced fractures and to keep the fractures opened after the fracturing process is complete. The second one is an engineered fluid system to transport these particles deep into the induced fracture. The solid and round particles used to keep the fracture open and conductive are defined as proppant.

Since the first hydraulic fracturing treatment was conducted in 1947¹, a variety of materials have been used as proppant, including rounded walnut shells, fused zirconia, plastic pellets, steel shot, glass beads, aluminum

pellets, fly ash proppants, silica sand, resin coated sand (RCS), ceramic and porous ceramic proppants, and thermoplastic alloys. Typical proppant size range lies between 105 μm to 2.38 mm or from 8 to 140 mesh. The most commonly used proppant sizes in the field are 16/30, 20/40, 30/50, 40/70, and 100 mesh². With more development in the unconventional resources, smaller mesh size proppants are used extensively to complete these wells.

Raw silica sand is among the most widely used materials as a proppant, meeting over 96.4% of the proppant demand reported in 2016. To increase the crush resistance strength of raw silica sand and improve the conductivity of the induced fracture, it is coated using different types of polymeric materials or resin, known as RCS or resin coated proppant (RCP)³. The third main category is that of man-made ceramic-based proppants, which are mostly made from sintered bauxite, kaolin, silicates or small aluminum beads, and were developed for reservoirs having high closure stresses³. Although the ceramic proppant has the highest crush resistance strength and provides the highest conductivity, it serves only 1.4% of proppant demand in the United States as reported in 2016⁴. Finally, the key factors that determine the proppant selection are the availability, raw materials cost, logistics, and economics of operation.

Ceramic proppant, being man-made, exhibits narrow particle size distribution close to singularity in sphericity and roundness scales, as its composition, size and shape can be engineered on a large scale. This gives the proppant a relatively very high crush resistance stress level among its peers. Ceramic proppant can be divided into three main categories; lightweight proppant, intermediate strength proppant, and high-density proppant. Palisch et al. (2014)⁵ evaluated the performance of different types of ceramic proppant. In addition to their high strength, ceramic proppants were further developed to offer multiple functionalities^{6,7} such as traceable proppants for fracture geometry⁸⁻¹², proppants that work as a carrier for scale and paraffin inhibitor^{10,13-17}, and proppants that serve as a carrier for breakers^{18,19}.

Sand, being a natural made material, exhibits noticeably large variations in its texture, composition, size, and shape, depending on the depositional environments, detrital sources and provenance. The nature of crystallinity, presence of impurities, and shape and size distributions influence the crush resistance stress level of the sand and provide an efficient conduit for the production of hydrocarbon. Two of the most widely used raw sands in hydraulic fracturing applications are the Northern white (NW) sand and Texas brown (Brady) sand. Naturally, NW sand is composed of quartz-rich, single crystalline, geologically mature grains with high sphericity and roundness resulting in a high crush strength, and is relatively more expensive¹⁹. Brady sand is polycrystalline in nature with a relatively larger presence of impurities and lags in roundness and sphericity when compared to NW sand.

Sand can be coated to further improve its crush resistance stress level, especially for applications where

sand needs to be exposed to higher stresses. Under stress exceeding the strength, crushing of sand generates fines that can block the pore space, which may result in reduced permeability and rapid production decline²⁰. Coating the sand with polymeric resin was found to reduce proppant crushing and fine generation, resulting in fractures with higher conductivities²⁰.

Among different types of coating chemistries, phenol formaldehyde resins (novolac and resole), epoxy, polyurethane, and furan resin are used extensively when it comes to RCS. For both resin systems, a hardener is added to complete the curing process or crosslinking reaction. In addition to the curing time and temperature, the molar ratio of the resin to the hardener defines the final properties of the RCS as well as its thermal stability²². RCP can be divided into two main categories: "curable" proppant where the resin will be gradually cured in a downhole condition, taking advantage of the reservoir temperature while the proppant sets in the fracture, and "pre-cured" where the RCP is fully cured in the proppant coating facility prior to being pumped^{23,24}.

In this work, we report a novel nanocomposite RCS having improved performance by introducing functional additives such as nano-reinforcement agents and surface charge altering agents compared to conventional resin coating technologies commercially known. For selection of a nano-reinforcing agent, a top-down approach was adapted, where instead of synthesizing the nanomaterials from a laboratory scale, commercially available products were screened for use as a proppant coating technology. Performance of the coated proppant, along with cost, logistics, and health and environmental safety (HSE) consideration were the key variables considered for developing this new material.

Experimental Study

Sphericity and Roundness

Sphericity and roundness measurements analyze the shape of particles. The higher the roundness (non-angularity) and sphericity (degree of which the particle approaches a spherical shape) indices, the higher will be the fracture conductivity. As defined by Krumbein and Schloss (1963)²⁵, sphericity and roundness need to be above 0.7 for a good proppant. In this method, an average of 20 particles are visually compared individually to Krumbein and Schloss' chart and numbered according to their sphericity and roundness scale.

An advanced technique is 3D optical scanning, which eliminates human error, and accurately measures the sphericity and roundness was implemented in this work.

Sieve Analysis

This test determines the particle size distribution of a proppant sample. As recommended in American Petroleum Institute (API) RP-19C, pre-weighted proppant particles are loaded in a stack of calibrated sieves. After 10 minutes of shaking, the weight percentage (wt%) of sand is calculated on each sieve. A minimum of 90% of the tested proppant sample should fall between the designated sieve sizes. Not over 0.1% of the total tested sample should be larger than the first sieve size, and not

Fig. 1 Proppant crush cell, pluviator, and Forney loading frame.



over 1.0% should fall on the pan. The in-size percent, mean particle diameter, and median particle diameter are calculated.

API Crush Resistance Stress Level Test

The crush resistance test was conducted following the protocol described at ISO 13503-2, using a Forney Model CA-0396 loading frame at room temperature. The main objective of this static test is to determine the amount of proppant, and therefore, the amount of fines generated, which will be crushed under static stresses. A pluviator has been used to minimize human error during loading sand into the crush cell, Fig 1. For the Forney loading frame, a software with “proppant” option has been installed to run the crush test automatically after loading the stainless steel crush cell containing the proppant sample. A simple way to ensure reproducibility between tests is to maintain the stress ramping rate constant at 2,000 psi/min before reaching the target stress level and maintaining it there a 2 minute hold time.

For RCP development, especially for curable proppant, relying on the crush resistance test alone can be misleading as proppant, i.e., ceramic and sand, responds and fails completely differently than resin or polymer

coated proppant under an applied load. The difference extends further when temperature and exposure to fluid is considered. The API crush test is a better evaluation tool for raw proppant — ceramic, and sand.

API Long-Term Conductivity Test

API long-term conductivity is the ultimate test the industry uses to benchmark proppant where the proppant pack is subjected to high closure stress in the presence of flowing fluid at a high temperature. The API long-term conductivity test has been conducted following the protocol described in ISO 13503-5. The test was conducted at a temperature of > 200 °F at successive closure stress of 2,000, 4,000, 6,000, 8,000, and 10,000 psi while the hold time at each stress was 50 hours. Tests were conducted using Ohio sandstone and a 2% potassium chloride (KCl) solution. Proppant loading was 2 lb/ft².

For RCP, the conductivity test provides further valuable information where damage to the resin coating, due to additional factors, such as high temperature and fracturing fluid exposure can be assessed. Due to the complexity and lengthy nature of the test, the error percentage for each measured conductivity in md-ft

Table 1 Relative comparison of API crush test and API long-term conductivity test.

	API Crush Strength Test	API Conductivity Test
Test Temperature	Room temperature	Up to 300 °F
Test Cell	Stainless steel	Ohio sandstone
Proppant Embedment	None	Realistic embedment
Test Time	~10-12 minutes	2 weeks continuous
Flow	None (dry condition)	2% KCl (wet and flow condition)

Table 2 Relative comparison between the two types of sands.

	NW Sand	Brady Sand
Quartz Type	Mostly plutonic grains	Mostly metamorphic grains
Crystalline Structure	Mostly monocrystalline	Mostly polycrystalline
Vacuoles Size	Very small	Relatively larger
Grain Boundaries	Less	Abundant
Impurities	Low	High (CuO, FeO)
Roundness	High roundness (> 0.8)	Poor roundness (~0.3 - 0.6)
Sphericity	High sphericity (> 0.8)	Poor sphericity (~0.3 - 0.6)
Maturity	Well sorted	Poorly sorted

can reach close to 30%. Table 1 highlights the relative distinctions between the API crush test and API long-term conductivity test.

Loss on Ignition (LOI) Test

Thermogravimetric analysis (TGA) was used in evaluating the quantity of resin coating on a sand substrate. During the coating process, not all the coating chemicals end up on the proppant substrate. Depending upon curing temperature, mixer type, mixing energy, among others, some chemicals are wasted on mixing blades and the vessel walls.

To quantify the amount of the coating chemicals on sand substrate, a small quantity of coated sand, typically ~20 mg to 40 mg, is heated from room temperature to 1,000 °C at 10 °C/min. The polymeric organic chemicals are burned at this high temperature leaving the original silica core. During the heating process, weight loss and heat flow is measured as a function of temperature to calculate the LOI, which is the amount of coating chemical estimated to be adhered to the proppant substrate. Alternatively, a larger sample of 10 mg of coated sand was heated in a vacuum over to 1,000 °C, and the measured difference in weight was an indication of the LOI.

Materials

A phenol formaldehyde (novolac) resin-based coating

was used to coat sand, which was further enhanced by introducing nanoscale reinforcement and surface wettability altering (WA) agents. A coupling agent and crosslinking agent were also used. As nano-reinforcement filler, a carbon nanotube-based nano-dispersion was introduced to the novolac resin. For surface wettability modification, a fluoro-alkyl functional agent was used²⁶.

Results and Discussion

Sand Analysis

“Not all sands are the same.” Quartz can be classified into plutonic, volcanic, vein, and metamorphic (recrystallized, schistose, stretched), depending on its distinct characteristics. Petrographic evaluation of different quality sands reveals wide variations ranging from a high presence of plutonic monocrystalline grains for high quality grains to polycrystalline and metamorphic grains having inner grain boundaries for lower quality sands.

Petrographic images were compared between NW and Brady sands on the basis of quartz type, crystalline structures, purity, sphericity, roundness, and sorting. Table 2 draws a qualitative comparison between the two types of sands. Figures 2 and 3 shows a set of petrography images for 30/50 mesh NW and Brady sands, respectively. The marked areas in the Brady sand shows the abundance of polycrystalline and metamorphic type quartz, whereas most of the grains in the NW sands

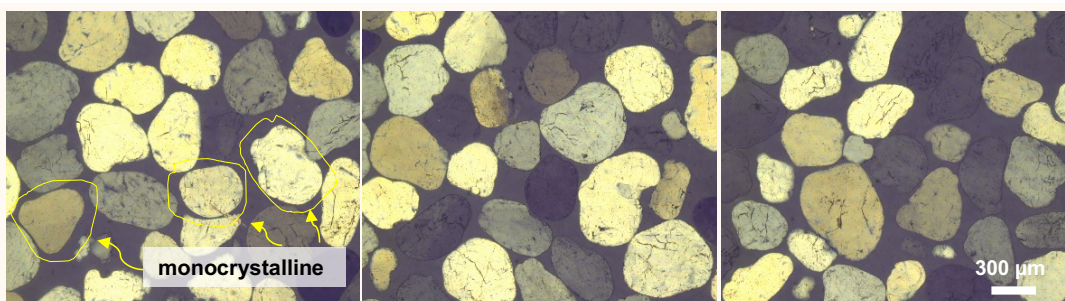
Fig. 2 Petrography image of 30/50 mesh NW sand (single crystal and plutonic quartz).

Fig. 3 Petrography image of 30/50 mesh Brady sand (polycrystalline, metamorphic grains are marked).

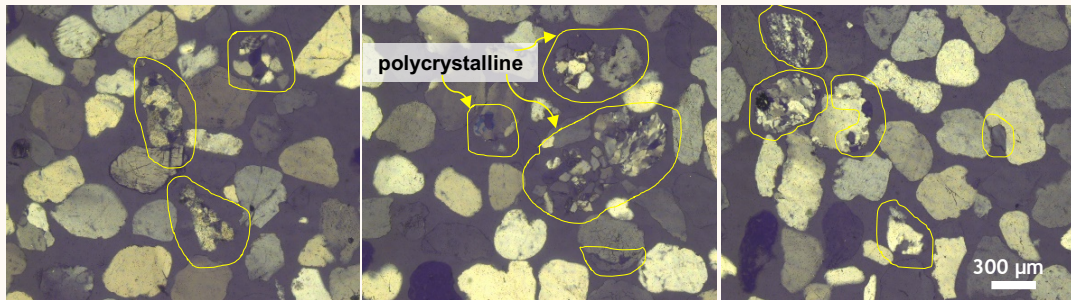
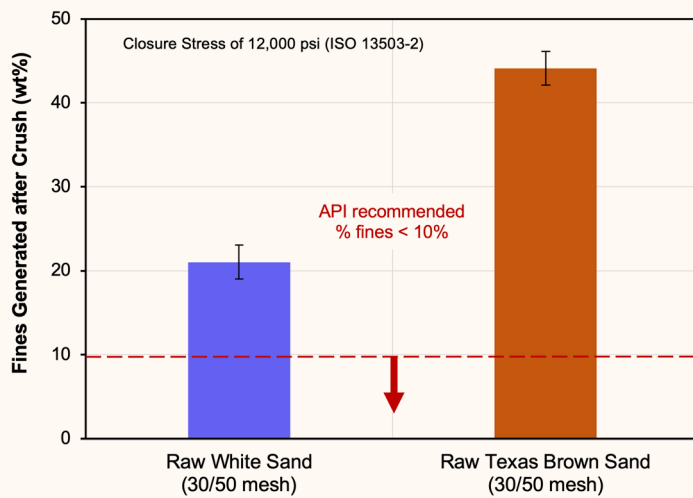


Fig. 4 Comparing the results of the crush resistance stress test for uncoated NW and Brady sands.



are of single crystal and plutonic type. As expected, in the API crush resistance stress test, the 30/50 mesh NW sand generates much less fines, Fig. 4. At a closure stress of 12,000 psi, the Brady sand generates almost twice as many fines.

XRF and XRD Analysis

X-ray fluorescence (XRF) is a nondestructive analytical technique used to determine the elemental composition of the NW and Brady sand as summarized in Table 3. Both contain > 99% quartz with the Brady sand showing an additional presence of impurities such as Fe_2O_3 , CuO , and K_2O . X-ray diffraction (XRD) is another analytical technique used to identify the phase of crystalline materials. Table 4 summarizes the results for the two types of sands. For XRF, Bruker S8 TIGER ECO wavelength-dispersive X-ray fluorescence (WDXRF) and for XRD, Bruker D8 ADVANCE were used.

Sphericity and Roundness (3D Scanning Analysis)

A relatively newer technique is to use 3D optical scanning of a collection of particles as they fall from a vibrating

stage at a defined rate. Figure 5 shows the results of 30/50 mesh NW sand measured in this technique for a population of 68,691 sand particles. The boxed top-right corner shows the sand population having a roundness of > 0.6, and a sphericity of > 0.85. The measured sphericity was 0.96 (standard deviation = 0.02) and the roundness was 0.64 (standard deviation = 0.09). Among proppant selection criteria, roundness plays a higher importance over sphericity for better management of stress distribution and providing a higher crush resistance stress level.

Single Grain Crush Test

The effect of sphericity has been quantified by a single grain crush test on sands having two different angularities, Fig. 6. One spherical (top left) and one elliptical (bottom left) sand grain from 20/40 mesh sands were placed between two compression platens in an Instron 5966 loading frame. As observed, the spherical grain sustained a load about three times higher, while absorbing about eight times higher energy. The observed failure modes were also distinct for the two cases captured by high-speed camera at 90,000 frames per second.

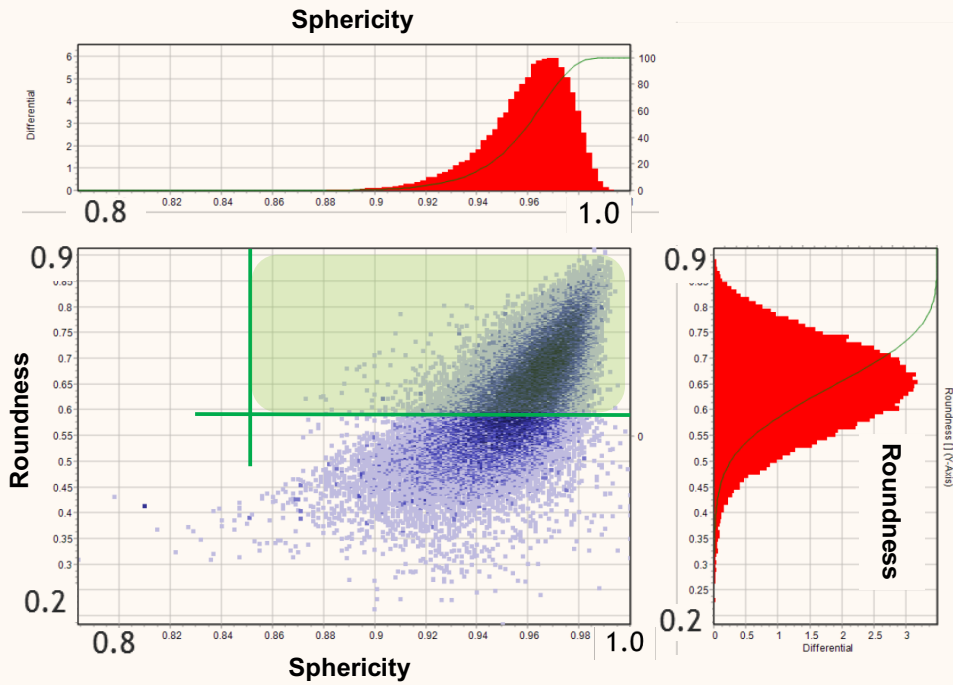
Table 3 XRF analysis of different sand samples.

Component	NW Sand	Brady Sand
SiO_2	99.773%	99.172%
Fe_2O_3	0.204%	0.472%
CuO	0.029%	0.337%
K_2O	—	0.019%

Table 4 XRD analysis of different sand samples.

Sand Type	Quartz	Kspar (KAISi_3O_8)
NW Sand	100%	0%
Brady Sand	97%	3%

Fig. 5 3D images analysis to characterize sphericity and roundness of 30/50 mesh NW sand particles (Courtesy: microtrac).



While the spherical grain exhibited sudden shattering, the angular grain gradually broke into smaller pieces generating the saw-teeth pattern in the load displacement plot, Fig. 6. The inset image in the plot in Fig. 6 captured the moment, showing a parting of the elliptical grain, immediately after the peak load of 27 Newtons was

exceeded, followed by two more peaks before the grain completely shattered as well. A change in load profile was observed, for the spherical grain, at around 50 Newtons and 40 μm of deformation, which could possibly be because of the onset of a crack initiation within the grain itself. The findings quantitatively confirm the higher

Fig. 6 Single grain crush test for 20/40 mesh sands having different angularities.

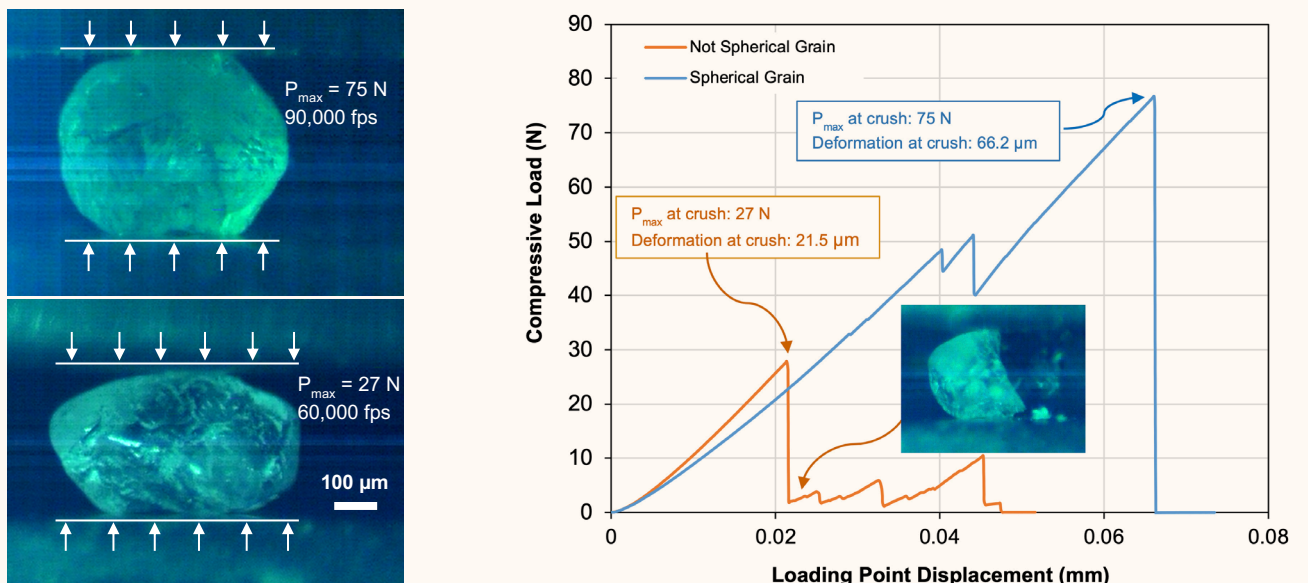


Fig. 7 Qualitative comparison of the API crush resistance stress level of raw and coated sand (not to scale).

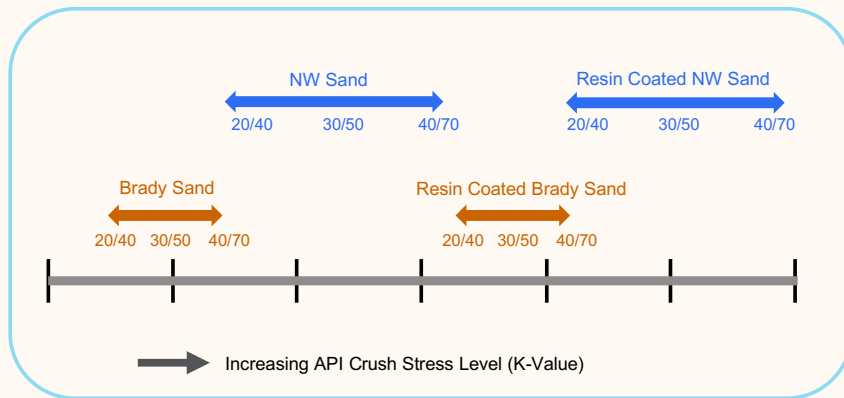
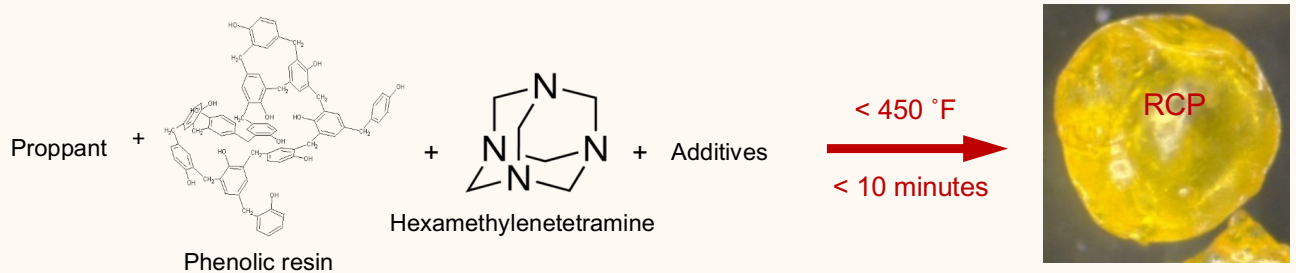


Fig. 8 Fundamentals of the coating formulation for the RCP.



load bearing capacity of spherical and rounder grains over grains having a poorer sphericity and roundness.

Effect of Resin Coating

Resin coating of proppant or sand is a well-established technology to increase its crush resistance stress level. The coating covers the proppant/sand substrate hiding its sharp edges and distributes the applied stress on the proppant pack uniformly. The polymeric coating contains the fines generated after the closure stress exceeds the crush strength of the sand packs. Therefore, the need for a strong polymeric coating that can adhere to the proppant substrate as well as contain the crushed fines from being released to the fracture is critical. Figure 7 draws a qualitative comparison of the API crush resistance stress level for NW and Brady sand when raw and coated under the same conditions. As evident, for weaker sand, the need for a stronger coating becomes more important, especially for the application at high closure stress. Mesh size has a measurable impact on its crush performance as a pack of smaller grains distribute stress better than a pack of larger grains.

Proppant/Sand Coating Process

Figure 8 illustrates a general description of the sand coating formulation where phenol formaldehyde (novolac) resin is cross-linked by hexamethylenetetramine at an

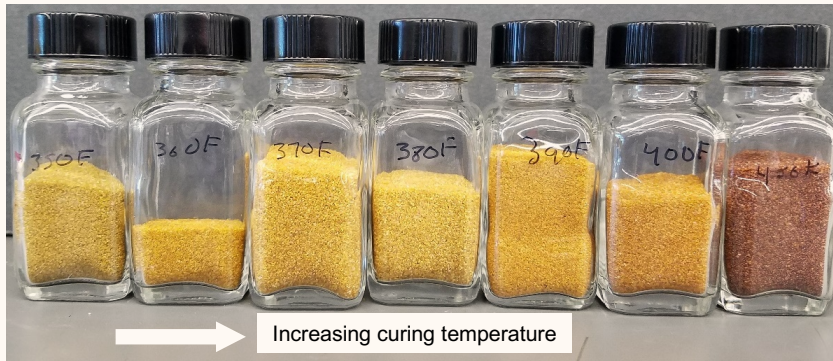
elevated temperature in the presence of functional additives. A pre-cured phenolic (novolac) resin can provide relatively higher glass transition temperature. The following variables were taken into consideration to optimize the sand coating process:

- Formaldehyde (CH_2O) to phenol ($\text{C}_6\text{H}_5\text{OH}$) molar ratio
- Melt viscosity of resin
- Curing temperature
- Heating/Cooling rate
- Resin to crosslinker ratio
- Curing temperature
- Type and dose of coupling agent
- Crosslinking reaction time
- Residence time of each additive and corresponding temperature hold time
- Dilutions for the additives
- Cooling media

Once coated properly, the quality of the RCS was evaluated by the following tests:

- Sphericity and roundness of finished product
- Optical microscopy

Fig. 9 RCS color gradient as a function of curing temperature. Increasing the curing temperature results in an increase in the “degree of curability” and gradually changes from a yellowish color to a brownish color.



- Degree of curability (acetone leaching test)
- LOI
- API crush resistance stress test
- API long-term conductivity

Degree of Curability

This important variable distinguishes the difference between the pre-cured and curable RCS. The degree of curability is a direct function of balancing the curing time and temperature. As illustrated in Fig. 9, the color of coated sand that was cured for a longer time at a higher temperature gradually turns to a brown color from a yellow color. A simple test to screen for the degree of curability is to expose the RCS in an acetone solution while looking for any change in color of the solvent. The degree of curability needs to be carefully controlled as an under-cured coating remains soft and doesn't provide the strength needed for the application, whereas an over-cured coating could introduce brittleness and at the same

time, could increase the overall coating cycle.

LOI

Figure 10a shows the weight loss profile of RCS measured in a TGA. In this case, the LOI was measured to be 3.12 wt%. Maintaining a suitable amount of coating on the proppant is very important. A less than optimal coating amount, Fig. 10b, may result in a low crush resistance stress level; whereas an excessive coating potentially reduces the inter-grain pore space and increases the mesh size of the finished product.

Nano-reinforcement of Resin Coating

Reinforcing the phenolic resin by mixing in a multi-walled carbon nanotube (MWNT) dispersion resulted in an enhancement in proppant performance. The MWNTs were screened based on the following properties:

- Diameter
- Aspect ratio

Fig. 10 The LOI data of RCS (a), and (b) a microscopic optical image of RCS.

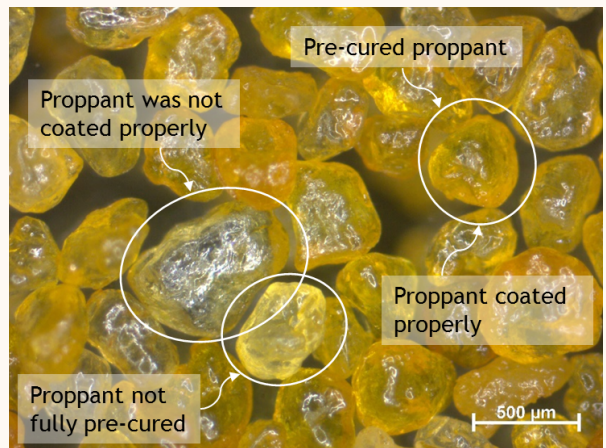
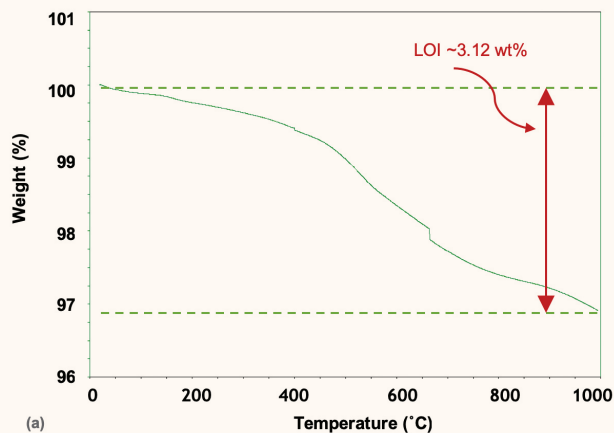
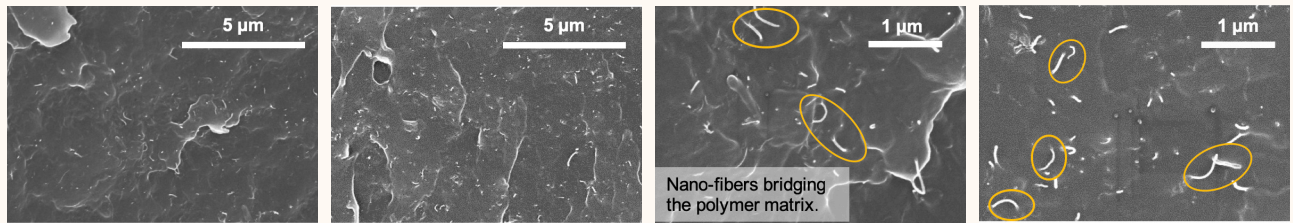


Fig. 11 An example of nanoscale MWNT fibers dispersed in a polymer matrix. A few of the MWNT fibers bridging the polymer matrix are marked in high resolution SEM images.



- Purity
- Density
- Brunauer-Emmett-Teller (BET) surface area analysis
- Viscosity
- Phase (dry solid, liquid)
- Dispersibility
- Cost/volume

MWNT dispersion with a very high aspect ratio ($> 12,000$) and BET surface area ($> 400 \text{ m}^2/\text{g}$) was blended in the resin matrix while maintaining the curing temperature, and with the total coating cycle unchanged. In principle, having well dispersed nanoscale MWNT fibers with an extremely high aspect ratio, acts like a bridge that holds the resin matrix providing additional mechanical strength. An improvement in resistance to chemical exposure at an elevated temperature has also been observed by an acetone leaching test. Figure 11 shows scanning electron microscope (SEM) images of

a MWNT dispersed polymer matrix where nanoscale fiber-like structures were seen to be heading out of a polymer matrix.

Reproducibility of the nanomaterials and the coating process were ensured after a series of tests performed on over 600 batches of RCS prepared in the laboratory. Cost, the phase of MWNT (dry powder vs. liquid dispersion), and HSE measures were carefully evaluated before scaling up of the coating technology from the lab to plant scale.

API Crush Resistance Stress Level

Figure 12 shows the API crush resistance stress test conducted on 30/50 mesh and 40/70 mesh uncoated raw sand, RCS, and nano-reinforced RCS (nano-RCS). The percentage of fines generated corresponds to a closure stress of 12,000 psi for each of the cases. The closure stress of 12,000 psi clearly exceeds the crush resistance stress level of the sand pack in the crush cell. Because of the smaller size and an increase in surface area, this leads to an increase in the number of point contacts between the sand particles. The 40/70 mesh sand pack undergoes a relatively better stress distribution, and generated less fines than the 30/50 mesh sand for each of the three cases. Though the impact of the coating on the generated fines were clearly observed, the impact of nano-RCS cannot be distinguished in this API crush strength test.

Effect of Nano-reinforcement on API Long-Term Conductivity Test Results

Unlike in the API crush strength test, the impact of nano-reinforcement on the RCS was observed and measured by API long-term conductivity testing²⁶. Figure 13 shows the normalized API long-term conductivity test results for the 30/50 mesh and 40/70 mesh uncoated raw sand, RCS, and nano-RCS. All six cases of data were normalized with respect to the 30/50 mesh nano-RCS data. For the 30/50 mesh sand, the measured conductivity of RCS and nano-RCS were 130% and 244% higher than raw sand, respectively. For the 40/70 mesh sand, the measured conductivity of RCS and nano-RCS were 41% and 100% higher than raw sand, respectively. For the raw sand, the 40/70 mesh sand showed a higher conductivity, whereas for the RCS and the nano-RCS, the 30/50 mesh sand showed a higher conductivity.

Fig. 12 Generated wt% of fines following ISO 13503-2 protocol for raw sand, RCS, and nano-RCS.

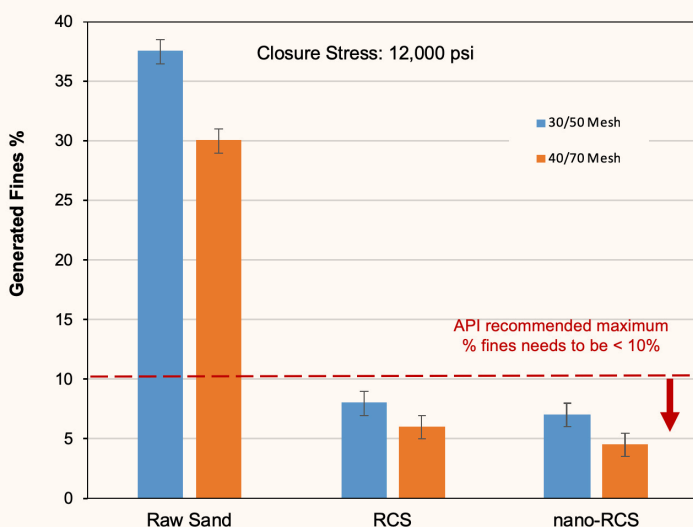


Fig. 13 Normalized API long-term proppant conductivity data (with respect to 30/50 mesh nano-RCS following ISO 13503-5 protocol for raw sand, RCS, and nano-RCS. Percentage increase in conductivity is calculated with respect to raw sand.

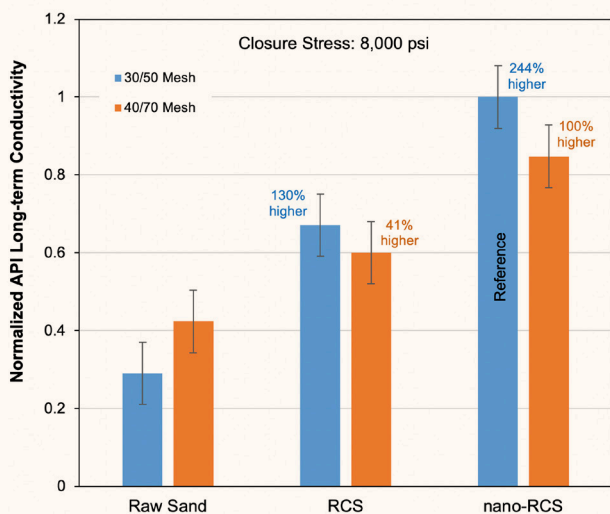
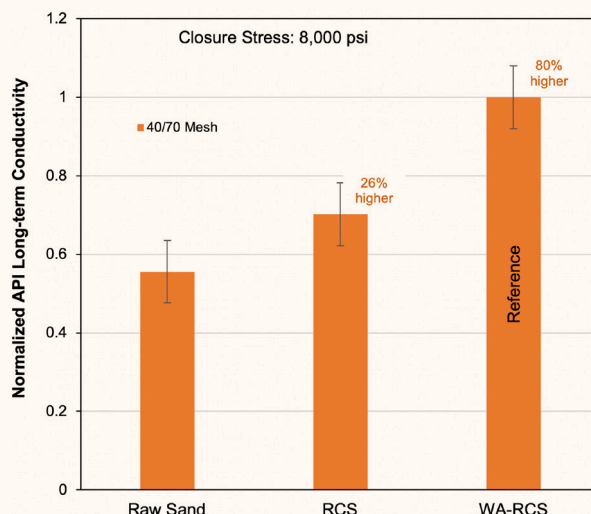


Fig. 14 Normalized API long-term proppant conductivity data (with respect to the 40/70 mesh WA-RCS) following ISO 13503-5 protocol for raw sand, RCS, and WA-RCS. The percentage increase in conductivity is calculated with respect to raw sand.



Effect of Surface WA on API Long-Term Conductivity Test Results

In a similar way, the impact of the surface WA of the RCS was clearly captured in the API long-term conductivity test, whereas the API crush strength test was not able to detect any change in the surface wetting property. This is simply because the API conductivity test accommodates the option to study the effect of changes in the surface wetting property as a 2% KCl solution is pumped through the proppant pack. Figure 14 shows the normalized API long-term conductivity test results for 40/70 mesh uncoated raw sand, RCS, and RCS with surface WA-RCS. All three cases of data were normalized with respect to the 40/70 mesh WA-RCS data. For the 40/70 mesh sand, the measured conductivity of RCS and WA-RCS were 26% and 80% higher than raw sand, respectively²⁵.

While comparing Fig. 13 and Fig. 14, it is observed that the 40/70 mesh RCS has a 41% vs. 26% increase in long-term conductivity with respect to raw sand of the same mesh. The reported test results in Fig. 13 and Fig. 14 were conducted in two different testing laboratories under identical conditions. This difference of 15% between the two test cases falls within the expected percentage of error (typically ~20%) observed in the measurement of the API long-term conductivity test as marked with the error bars in the respective plots.

Conclusions

In summary, sand, as a core material, and resin as a coating material, were investigated using laboratory techniques, which included sphericity and roundness analysis, size distribution, mineral composition, petrography, single grain crush test, LOI, and standard ISO tests such as the API crush resistance stress, and API long-term proppant conductivity tests. We report an

enhancement of the proppant pack conductivity performance by introducing nano-reinforcing MWNT fibers and a WA agent to the RCS as measured by API long-term proppant conductivity.

For nano-reinforcement, the measured conductivity of the RCS and nano-RCS were 130% and 244% higher than equivalent 30/50 mesh uncoated sand, respectively. For the 40/70 mesh sand, the measured conductivity of the RCS and nano-RCS were 41% and 100% higher than uncoated sand, respectively. With surface WA, we have measured an 80% increase in API long-term conductivity for the 40/70 mesh compared to an equivalent 40/70 mesh uncoated sand. The impact of the nanomaterials in the coating process were successfully reproduced while considering the economics and HSE concerns as well as the potential scalability of the coating technology from lab to plant scale.

Acknowledgments

The authors would like to thank the management of Saudi Aramco and Aramco Services Company for their support and permission to publish this article. The authors would also like to acknowledge David Jacobi of the Reservoir Engineering Team and Prof. Younane Abousleiman of University of Oklahoma for their valuable input. In addition, the authors also would like to thank Brent Cooper and Shahrazed Metouri for their help with the sample preparation and laboratory testing.

This article was presented at the Offshore Technology Conference, Houston, Texas, May 6-9, 2019.

References

- Montgomery, C.T. and Smith, M.B.: "Hydraulic Fracturing: History of an Enduring Technology," *Journal of Petroleum Technology*, Vol. 62, Issue 12, February 2015, pp. 26-40.

2. Mittal, A., Rai, C. and Sondergeld, C.: "Experimental Proppant Conductivity Observations: Evaluating Impact of Proppant Size and Fluid Chemistry on Long-Term Production in Shales," SPE paper 191741, presented at the SPE Annual Technical Conference and Exhibition, Dallas, Texas, September 24-26, 2018.
3. Gallagher, D.G.: "The Hierarchy of Oily Conductivity," *Journal of Petroleum Technology*, Vol. 63, Issue 4, April 2011, pp. 18-19.
4. The Freedonia Group: "Proppants Market in North America," Industry Study #3535, July 2017, 122 p.
5. Palisch, T., Wilson, B. and Duenckel, R.J.: "New Technology Yields Ultra High-Strength Proppant," SPE paper 168631, presented at the SPE Hydraulic Fracturing Technology Conference, The Woodlands, Texas, February 4-6, 2014.
6. Saldungaray, P., Palisch, T. and Leasure, J.: "Can Proppants Do More Than Hold the Fracture Open?" SPE paper 177978, presented at the SPE Saudi Arabia Section Annual Technical Symposium and Exhibition, al-Khobar, Saudi Arabia, April 21-23, 2015.
7. Radwan, A.: "A Multifunctional Coated Proppant: A Review of Over 30 Field Trials in Low Permeability Formations," SPE paper 187329, presented at the SPE Annual Technical Conference and Exhibition, San Antonio, Texas, October 9-11, 2017.
8. Duenckel, R.J., Smith, H.D., Warren, W.A. and Grae, A.D.: "Field Application of a New Proppant Detection Technology," SPE paper 146744, presented at the SPE Annual Technical Conference and Exhibition, Denver, Colorado, October 30-November 2, 2011.
9. Grae, A.D., Duenckel, R.J., Nelson, J.R., Smith, H.D., et al.: "Field Study Compares Fracture Diagnostic Technologies," SPE paper 152169, presented at the SPE Hydraulic Fracturing Technology Conference, The Woodlands, Texas, February 6-8, 2012.
10. Goyal, S., Raghuraman, A., Aou, K., Aguirre-Vargas, E., et al.: "Smart Proppant with Multiple Downhole Functionalities," SPE paper 184853, presented at the SPE Hydraulic Fracturing Technology Conference and Exhibition, The Woodlands, Texas, January 24-26, 2017.
11. Dal Forno, L., Latronico, R., Saldungaray, P., Petteruti, E., et al.: "Non-Radioactive Detectable Proppant First Applications in Algeria for Hydraulic Fracturing Treatments Optimization," SPE paper 175811, presented at the SPE North Africa Technical Conference and Exhibition, Cairo, Egypt, September 14-16, 2015.
12. Zhang, P., Sen, M.K., Sharma, M.M., Gabelmann, J., et al.: "Modeling of Low-Frequency Downhole Electrical Measurements for Mapping Proppant Distribution in Hydraulic Fractures in Cased Hole Wells," *SPE Journal*, Vol. 23, Issue 6, December 2018, pp. 2147-2157.
13. Satyanarayana Gupta, D.V. and Kirk, J.W.: "Method of Inhibiting or Controlling Formation of Inorganic Scales," U.S. Patent No. 7,491,682, 2009.
14. Szymczak, S., Brown, J.M., Noe, S. and Gallup, G.: "Long-Term Scale Inhibition Using a Solid Scale Inhibitor in a Fracture Fluid," SPE paper 102720, presented at the SPE Annual Technical Conference and Exhibition, San Antonio, Texas, September 24-27, 2006.
15. Brown, J.M., Satyanarayana Gupta, D.V., Taylor, G.N., Shen, D., et al.: "Laboratory and Field Studies of Long-term Release Rates for a Solid Scale Inhibitor," SPE paper 140177, presented at the SPE International Symposium on Oil Field Chemistry, The Woodlands, Texas, April 11-13, 2011.
16. Satyanarayana Gupta, D.V. and Kirk, J.W.: "Well Treatment Compositions for Slow Release of Treatment Agents and Methods of Using the Same," U.S. Patent No. 7,493,955, 2009.
17. Szymczak, S., Satyanarayana Gupta, D.V., Steiner, W., Bolton, S., et al.: "Well Stimulation Using a Solid, Proppant-Sized, Paraffin Inhibitor to Reduce Costs and Increase Production for a South Texas, Eagle Ford Shale Oil Operator," SPE paper 168169, presented at the SPE International Symposium and Exhibition on Formation Damage Control, Lafayette, Louisiana, February 26-28, 2014.
18. Duenckel, R.J.: "Proppants for Gel Clean-Up," U.S. Patent No. 7,721,804, 2010.
19. Duenckel, R.J., Leasure, J.G. and Palisch, T.: "Improvements in Downhole Chemical Delivery: Development of Multifunctional Proppants," SPE paper 168605, presented at the SPE Hydraulic Fracturing Technology Conference, The Woodlands, Texas, February 4-6, 2014.
20. Stephenson, C.J., Rickards, A.R. and Brannon, H.D.: "Is Ottawa Still Evolving? API Specifications and Conductivity in 2003," SPE paper 84304, presented at the SPE Annual Technical Conference and Exhibition, Denver, Colorado, October 5-8, 2003.
21. Liang, F., Sayed, M., Al-Muntasheri, G.A., Chang, F.F., et al.: "A Comprehensive Review on Proppant Technologies," *Petroleum*, Vol. 2, Issue 1, March 2016, pp. 26-39.
22. Dewprashad, B., Abass, H.H., Meadows, D.L., Weaver, J.D., et al.: "A Method to Select Resin Coated Proppants," SPE paper 26523, presented at the SPE Annual Technical Conference and Exhibition, Houston, Texas, October 3-6, 1993.
23. Murphey, J.R. and Totty, K.D.: "Continuously Forming and Transporting Consolidatable Resin Coated Particulate Materials in Aqueous Gels," U.S. Patent No. 4,829,100, 1989.
24. Underdown, D.R., Day, J.C. and Sparlin, D.D.: "A Plastic Pre-Coated Gravel for Controlling Formation Sand," SPE paper 8801, presented at the Formation Damage Control Symposium, Bakersfield, California, January 28-29, 1980.
25. Krumbein, W.C. and Sloss, L.L.: *Stratigraphy and Sedimentation*, 2nd edition, San Francisco: Freeman and Company, 1963, 600 p.
26. Haque, M.H., Saini, R.K. and Sayed, M.A.: "Nanocomposite Coated Proppant and Methods of Making and Use," U.S. Patent Application No. 62/671,183, 2018.

About the Authors

Dr. Mohammad H. Haque

Ph.D. in Materials Science & Engineering, University of Texas at Dallas

Dr. Mohammad H. Haque joined the Production Technology Team at the Aramco Research Center-Houston as a Petroleum Engineer in 2016. Previously, he worked with the Reservoir Engineering Team at the Aramco Research Center-Boston, beginning in 2013. Mohammad has more than 15 years of experience in nanotechnology, applied materials and mechanical engineering R&D. He specializes in nanocomposites and applied materials technologies, including lightweight structures, fiber reinforced polymer matrix composite, proppant coating, micro/nano-fractures in rock, smart materials and structures, artificial muscles, nano/micro-actuators with direct contributions from lab to scale up and commercialization.

Prior to working at Aramco, Mohammad was the Practice Leader at the Fraunhofer Technology Development Group (currently Fraunhofer Institute for Manufacturing Engineering and Automation) in Stuttgart, Germany. He led two European Commission (Sixth Framework Program) and over 20 small- to mid-sized enterprise sponsored projects developing nanomaterials based customized

applications and prototypes. Mohammad was the key account manager of a Fraunhofer spin-off in the U.S. devoted to prototype development and commercialization. He has close interactions with aerospace, automotive, bio-medical, composites, textile, sports, and oil and gas industries in Europe, and the U.S.

Mohammad has authored 16 papers in peer-reviewed journals, including *Science*, *Carbon*, *Composite Structures*, and *Composite Science and Technology*. He holds three granted patents and has over six pending applications.

Mohammad received his B.S. degree in Mechanical Engineering from the Bangladesh University of Engineering & Technology (BUET), Dhaka, Bangladesh, and his M.S. degree in Computational Mechanics from the University of Stuttgart, Stuttgart, Germany. Mohammad also received an M.S. and Ph.D. degree in Materials Science & Engineering from the University of Texas at Dallas, Dallas, TX.

In 2000-2001, he taught Mechanical Engineering courses as a lecturer at BUET.

Dr. Rajesh K. Saini

Ph.D. in Organic Chemistry, Kurukshetra University

Dr. Rajesh K. Saini is a Research Science Specialist in the Production Technology Team at the Aramco Research Center-Houston. He has more than 22 years of experience in the oil and gas industry, and chemical research. Rajesh is a subject matter expert in oil field stimulation, production and operations technology. He specializes in product development, scaling up, intellectual property, sales and commercialization of new products/processes for hydraulic fracturing, sand control, acidizing, production technology, oil field chemicals, and water conformance. Prior to joining Aramco in 2017, Rajesh played critical roles at Halliburton, Weatherford, and Lubrizol in the capacity from Research Scientist to R&D Manager.

He has served as a technical reviewer for major journals, including the *Journal of American Chemical Society*, and the *Journal of Organic Chemistry and Organic Letters*. Rajesh is a Technical Editor for the Society of Petroleum Engineers (SPE) *Production and*

Operations Journal. He is serving on the SPE Annual Technical Conference and Exhibition (ATCE) well stimulation committee. Rajesh holds 54 U.S. patents, 21 U.S. patent applications, and has published one book chapter and 48 peer-reviewed journal articles.

He served as the Distinguish Lecture's Program Chair and Director of the SPE-Southwest Oklahoma Section during 2009-2012. Rajesh received the Maximizing Value-Added Performance (MVP) Award at Halliburton for developing environmental fracturing fluid (CleanStim[®]) and breaker for AquaLinear[®] fluid. In 2018, he was also awarded the SPE Gulf Coast Regional award for Production and Operations.

Rajesh received his MBA from Oklahoma State University, Stillwater, OK, and his Ph.D. degree in Organic Chemistry from Kurukshetra University, Haryana, India. He was a postdoctoral fellow at Rice University working with Prof. W.E. Billups and Richard E. Smalley (Nobel Laureate in Chemistry).

Dr. Mohammed A. Sayed

Ph.D. in Petroleum Engineering, Texas A&M University

Dr. Mohammed A. Sayed joined the Production Technology Team at the Aramco Research Center-Houston as a Research Scientist in 2013. In this role, he is working to develop new chemical treatments and fluids used in acidizing carbonate reservoirs (matrix acidizing and acid fracturing). Mohammed is also creating new fluids utilized for hydraulic fracturing in both conventional and unconventional reservoirs, acidizing additives and wettability alteration chemicals, as well as developing new solutions for gas hydrate removal and mitigation, and investigating the productivity decline in unconventional oil and gas resources. He is also responsible for assisting in the preparation and follow-up on programs for workover operations, well testing, well acidizing and stimulation treatments, as well as

preparing reports on assigned projects or programs in the oil field operations.

Mohammed is a contributor to technical papers and is a member of the Society of Petroleum Engineers (SPE) as well as the American Chemical Society (ACS). He has presented at various industry conferences, including the Offshore Technology Conference (OTC), Middle East Oil and Gas Show (MEOS), and the International Conference on Oil Field Chemistry, as well as publishing peer-reviewed papers in the *Canadian Journal of Petroleum Technology*, *SPE Production and Operation Journal* and *Advances in Water Resources*.

Mohammed received his Ph.D. degree in Petroleum Engineering from Texas A&M University, College Station, TX.